Dynamics of salt intrusion in complex estuarine networks; an idealised model applied to the Rhine-Meuse Delta

Bouke Biemond[1], Wouter Kranenburg[2,3], Ymkje Huismans[2,3], Huib E. de Swart[1], and Henk A. Dijkstra[1]

[1]Institute for Marine and Atmospheric research Utrecht, Department of Physics, Utrecht University, Utrecht, the Netherlands
[2]Marine and Coastal Systems, Deltares, Delft, the Netherlands
[3]Faculty of Civil Engineering and Geosciences, Delft University of Technology, Delft, The Netherlands

Correspondence: Bouke Biemond (w.t.biemond@uu.nl)

Abstract. Many deltas in the world consist of a network of connected channels. We identify and quantify characteristics of salt intrusion in such systems with use of an idealised model. The Rhine-Meuse Delta is selected as a prototype example of a complex network with many channels. The model is able to capture the characteristics of the tide-dominated water level variations due to the main tidal component and the salinity time series for one year of observations. Quantification of tidally averaged salt transport components shows that transport related to exchange flow is dominant in the seaward, deep parts of the network, but tidal dispersion is dominant in shallower channels further inland. Close to the network junctions, a tidally averaged downgradient salt transport is generated by the tidal currents, which is explained from the phase differences between the tidal currents in the different channels. Salt overspill is confined to the most seaward part of the Rhine-Meuse Delta. The magnitudes of the response times of different channels to changes in discharge increases with distance to the estuary mouth, and with decreasing net water transport through the channel. In channels without a subtidal discharge, response times are a factor 2-4 larger than in the other channels. The effect of changes to the depth on the extent of salt intrusion strongly depends on where the change takes place. If the change is within the salt intrusion range, deepening will locally increase salt intrusion due to an increase in salt transport by the exchange flow. If the change is outside the salt intrusion range, changes to the net water transport dominate the response of the salt intrusion.

1 Introduction

The extent of salt intrusion in estuaries is changing worldwide, as a result of climate change and anthropogenic activities. Climate change includes e.g. sea level rise (Qiu and Zhu, 2015) and changes in freshwater discharge (Bellafiore et al., 2021). Examples of anthropogenic activities are dam constructions in rivers for water storage and hydropower generation (Qiu and Zhu, 2013), channel deepening for ship navigation and construction of polders (Liu et al., 2019). The availability of theoretical frameworks to explain, and suitable models to simulate salt intrusion, are crucial to predict how these changes affect the extent of salt intrusion.

For single-channel estuaries, relationships between estuarine geometry, forcing conditions and salt intrusion are extensively studied. For this, theoretical frameworks (Geyer and MacCready, 2014), semi-empirical models (Savenije, 1993), idealised

models (MacCready, 2004; Wei et al., 2022), models of intermediate complexity (Dijkstra and Schuttelaars, 2021) and detailed numerical models (Ralston et al., 2010; Martyr-Koller et al., 2017; Liu et al., 2024) are being used.

However, a number of estuaries consist of multiple channels. For these systems, also referred to as estuarine networks, the theories developed for single-channel estuaries need to be extended, as they behave differently in several ways. Observations show (Gong et al., 2014) that a tidally averaged salt transport between channels through the junctions occurs, a phenomenon known as salt overspill. Second, the phasing of tidal currents in estuarine networks creates local minima in the salt field (Warner et al., 2002; Garcia et al., 2022), which challenges the traditional view that salt transport by tides can be considered as a dispersive process (Winterwerp, 1983). The implications of these phenomena for the large-scale salt dynamics are hard to determine from observations. Furthermore, unsteadiness of the salt field is known to be important to single-channel estuaries (e.g. Bowen and Geyer (2003); Banas et al. (2004)). For estuarine networks, Biemond et al. (2023) find that the interaction between channels depends on forcing conditions. Observations show that salt intrusion in some channels in the Mekong Delta changes substantially due to variation in tidal forcing over the spring-neap cycle, while other channels are less sensitive (Eslami et al., 2021). Using a 3D model, they explained this from differences in depth and stratification, but the interaction between the channels was not explicitly quantified. Next, theory about the effect of changes to the geometry of estuaries does not contain all the relevant processes in estuarine networks. For example, Wu et al. (2016) suggest that deepening of the North Passage, one of the channels of the Yangtze River Estuary, may have contributed to salinity of the other channels. Liu et al. (2019) mention that channel deepening changed the amount of discharge reaching the Modoamen Waterway in the Pearl River Delta, but that local channel deepening was more important to the salt intrusion.

Salt intrusion in estuarine networks has been studied with one-dimensional (1D) models, e.g. by Nguyen and Savenije (2006) and Zhang et al. (2011). Such models, when calibrated, have proven to be successful in predicting salt intrusion in estuaries, but their simplified nature does not allow to identify the mechanisms of salt intrusion. On the other hand, three-dimensional (3D) models have been used (e.g. Xue et al. (2009); Bricheno et al. (2021); Bellafiore et al. (2021)), and while these models typically include a realistic geometry and a wide range of physical processes that affect the salt transport, their high computational costs makes extensive sensitivity studies computationally unfeasible. To fill the gap between simple 1D models and 3D numerical models of estuarine networks, we develop here an idealised, partly analytical, width-averaged (2DV) model. This model is suitable for a process-based analysis of salt intrusion mechanisms, as the model solves separately for different components of currents and salinity, which makes it straightforward to compute different components of the salt transport. Furthermore, it has lower computational costs than a 3D numerical model and it is e.g. easier to implement estuarine network geometry.

To study the characteristics of salt intrusion in estuarine networks, the model will be applied to the Rhine-Meuse Delta (the Netherlands) (RMD), which is formed by the outflow of the Rhine and Meuse rivers that discharge into the North Sea (Fig. 1). The current geometry of the delta is to a large extent anthropogenic determined (Cox et al., 2021), with the large harbour of Rotterdam situated in the seaward part. Earlier research on salt intrusion in this system by de Nijs and Pietrzak (2012), using measurements and 3D model simulations, revealed that intertidal transport of salt between the channels occurs, but effects of these transports on the tidally-averaged salinity were not quantified. Recently, salt intrusion in the RMD has received increased attention. Kranenburg et al. (2022) showed that upstream salt transport is dominated by exchange flow in the seaward part and
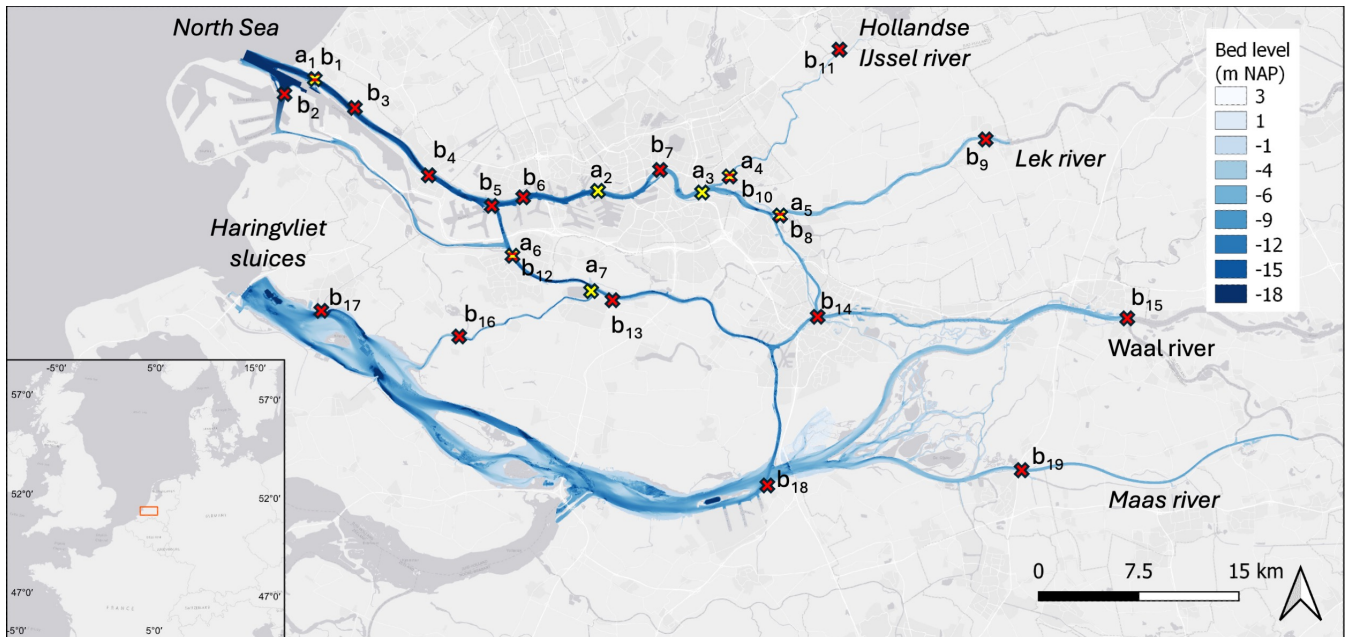
Figure 1. Map of the Rhine-Meuse Delta. The inset shows the location in Europe. The bed level is indicated in NAP, which is a measure of the mean sea level. The yellow crosses indicate salinity observation points (a_1-a_8) and the red crosses water level observation points (b_1-b_{19}). Locations where both these quantities are measured, or when these observation points are very close together, are indicated with both colours.

by tidal currents in the landward part of one of the major branches, but that during storm surges the relative importance of the different mechanisms changes. Wullems et al. (2023) point at the dependency of salinity on water level at one location in the network, using a data-driven method. None of these studies provide a network-wide analysis of salt intrusion.

To systematically investigate the dynamics of salt intrusion in estuarine networks, we formulate four specific aims: 1) Show that a calibrated idealised 2DV model successfully hindcasts hydrodynamics and salinity in an estuarine network. 2) Identify and quantify the different salt transport processes in an estuarine network, and highlight the differences with single-channel estuaries. 3) Quantify the time-dependent response to changes in discharge in an estuarine network. 4) Quantify the effects of changes to the depth of individual channels on salt intrusion in the major branches of an estuarine network.

The remainder of this manuscript is organised as follows. In Section 2, the model, its implementation in the RMD and the set-up of the simulations are described. Section 3 presents results focused on the four specific aims. Section 4 discusses the results and Section 5 presents the conclusions.

2 Model formulation

2.1 Model approach

The model chosen to address the research questions is an exploratory model. This type of model is simplified where possible, such that it only contains the essential ingredients to describe the relevant physics (Murray, 2003). The simplifications aim at isolating poorly understood phenomena, in this case salt intrusion in estuarine networks. An additional advantage is that, due to the lower computational demand, parameter sensitivity studies are easy to perform. Successful examples of this approach in the context of salt intrusion can be found in e.g. MacCready (2004), Chen (2015) and Wei et al. (2016). A detailed quantitative agreement with observations is not the primary goal of this type of models. However, to assure that the right part of the parameter space is investigated, we will calibrate the model parameters by a model-observations comparison. The simplifications in the model primarily concern the geometry, the turbulence closure, and disregarded physical processes. In the model description in the remaining of this section, simple formulations of these aspects will be used. The consequences of the assumptions on which these formulations are built will be addressed in the discussion section.

2.2 Domain

The domain mimics an estuarine network that has a number of width-averaged channels, which are connected to each other through a set of junctions. As a specific example, Fig. 2 shows the representation of the RMD network. There are four types of horizontal boundaries for the channels: river boundaries, weir boundaries, sea boundaries (estuary mouths), and junctions. Salt enters through the sea boundaries. Fresh water enters (or leaves, e.g. in the case of the Haringvliet sluices) through the river and weir boundaries. The junctions provide the connections between the channels.

Each channel i is divided in a number of segments j, which have different constant depths H_{ij}. Locations in the segments are characterised by a horizontal coordinate x_{ij}, which runs from $-L_{ij}$ to 0, and by a vertical coordinate z_{ij}, that runs from the bottom $z_{ij} = -H_{ij}$ to the water surface $z_{ij} = \eta_{ij}$, while the undisturbed water level is at $z_{ij} = 0$. By convention, x_{ij} increases in the direction of the time- and cross-sectionally averaged flow for yearly averaged discharge conditions (indicated with arrows in Fig. 2). For clarity, the subscript ij will be left out from now, and the equations shown are valid for each segment. The width of each segment is described as

$$b(x) = b(x = -L)e^{(x+L)/L_b}, \tag{1}$$

where L_b is an e-folding length scale which describes the width convergence. The width is continuous at the boundaries of the segments, but not necessarily at the junctions.

2.3 Equations of motion

The governing equations for hydrodynamics and salinity are described in Biemond et al. (2024a). In short, the model is width-averaged, and on this domain momentum and continuity balances are solved for hydrodynamics and a mass balance is solved for salinity. Water level η, horizontal and vertical velocity u and w, and salinity s are decomposed in tidally varying (indicated
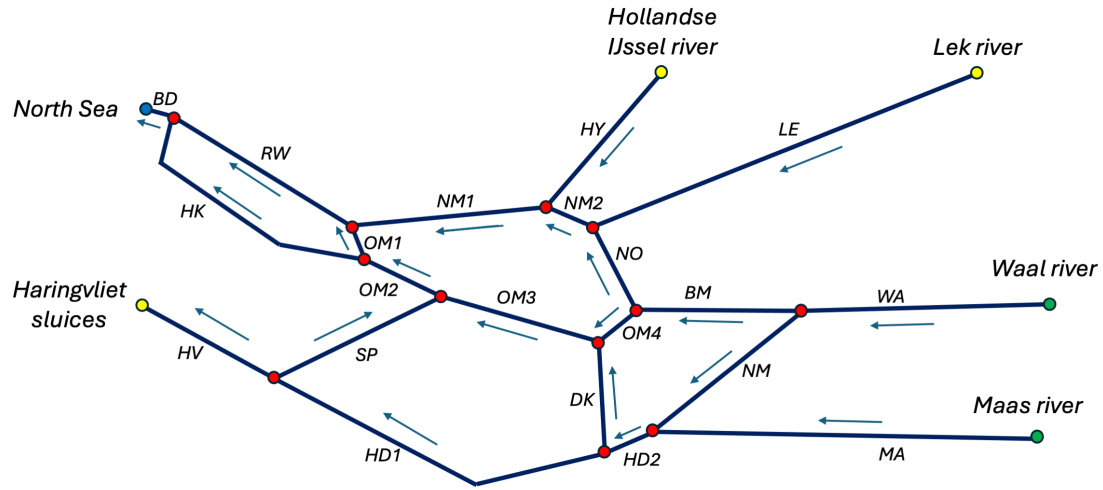
Figure 2. Representation of the RMD channel network in the model. Black lines indicate channels, blue arrows the direction of the local x-axis, red dots indicate junctions, yellow dots indicate weir boundaries, green dots indicate river boundaries, and blue dots indicate sea boundaries. Table A1 provides the meaning of the acronyms for the channels.

with subscript ti) and subtidal (indicated with subscript st) components. Subtidal horizontal velocity and salinity are further decomposed into a depth-averaged component (indicated with an overbar) and depth-dependent component (indicated with a prime). This yields

$$\eta = \eta_{st} + \eta_{ti}, \quad u = \bar{u}_{st} + u'_{st} + u_{ti}, \quad w = w_{st} + w_{ti}, \quad s = \bar{s}_{st} + s'_{st} + s_{ti}. \tag{2}$$

Analytical solutions to the dominant tidally averaged momentum and mass balances are found, which yield expressions for subtidal water level gradient $\frac{\partial \eta_{st}}{\partial x}$, the depth-averaged and depth-varying component of the subtidal horizontal velocity u_{st} and vertical velocity w_{st}. They read

$$\frac{\partial \eta_{st}}{\partial x} = -\frac{6}{5} \frac{A_{v,st} Q}{gbH^3}, \tag{3a}$$

$$\bar{u}_{st} = \frac{Q}{bH}, \tag{3b}$$

$$u'_{st} = \frac{Q}{bH} P_1(\tilde{z}) + \frac{g\beta H^3}{48 A_{v,st}} \frac{\partial \bar{s}_{st}}{\partial x} P_2(\tilde{z}), \tag{3c}$$

$$w_{st} = -\frac{g\beta H^4}{48 A_{v,st}} \left(\frac{\partial^2 \bar{s}_{st}}{\partial x^2} + L_b^{-1} \frac{\partial \bar{s}_{st}}{\partial x} \right) P_w(\tilde{z}). \tag{3d}$$

Here, Q is net water transport, $g = 9.81$ m s^{-2} is gravitational acceleration, $\beta = 7.6 \ 10^{-4}$ (g/kg)$^{-1}$ is the isohaline contraction coefficient, and $A_{v,st}$ is the vertical eddy viscosity acting on the subtidal flow. The quantity $\frac{\partial \eta_{st}}{\partial x}$ is required to calculate the water distribution over the channels, and similarly w_{st} is required for the vertical structure of the subtidal salinity field s'_{st}.

Note that we have neglected the contribution of salinity to the subtidal water level gradient, because taking it into account would introduce a strong relationship between salinity and net water transport, which is not realistic (Buschman et al., 2010; Maicu et al., 2018; Wang et al., 2021). Polynomials P_1, P_2 and P_w describe the vertical structure of the flow, and depend on normalised vertical coordinate $\tilde{z} = \frac{z}{H}$. They are defined as

$$P_1(\tilde{z}) = (\frac{1}{5} - \frac{3}{5}\tilde{z}^2), \quad P_2(\tilde{z}) = (\frac{8}{5} - \frac{54}{5}\tilde{z}^2 - 8\tilde{z}^3), \quad P_w(\tilde{z}) = (2\tilde{z}^4 + \frac{18}{5}\tilde{z}^3 - \frac{8}{5}\tilde{z}). \tag{4}$$

The water level η_{ti}, horizontal velocity component u_{ti} and vertical velocity component w_{ti} of the tidally varying flow field read

$$(\eta_{ti}, u_{ti}, w_{ti}) = \Re\{(\hat{\eta}_{ti}, \hat{u}_{ti}, \hat{w}_{ti})\exp(i\omega t)\}, \tag{5a}$$

$$\hat{\eta}_{ti} = \exp\left(-\frac{(x+L)}{2L_b}\right)(C_1\exp(k(x+L)) + C_2\exp(-k(x+L))), \tag{5b}$$

$$\hat{u}_{ti} = \frac{g}{i\omega}\frac{\partial\hat{\eta}_{ti}}{\partial x}\left(B\cosh(\delta_A\frac{z}{H}) - 1\right), \tag{5c}$$

$$\hat{w}_{ti} = i\omega\hat{\eta}_{ti} - \frac{g}{i\omega}\left(\frac{d^2\hat{\eta}_{ti}}{dx^2} + \frac{1}{L_b}\frac{d\hat{\eta}_{ti}}{dx}\right)\left(\frac{BH}{\delta_A}\sinh(\delta_A\frac{z}{H}) - z\right). \tag{5d}$$

Here ω is the angular frequency of the tidal constituent that is considered, t is time, L is the length of a channel segment, $\Re$ denotes the real part of a complex variable, and C_1 and C_2 are determined by the horizontal boundary conditions and represent tidal waves that travel downstream and upstream, respectively. The other parameters are defined as

$$\delta_A = \frac{(1+i)H}{\sqrt{\frac{2A_{v,ti}}{\omega}}}, \quad B = \left(\cosh(\delta_A) + \frac{\delta_A}{2}\sinh(\delta_A)\right)^{-1}, \quad k = \sqrt{\frac{1}{(2L_b)^2} + \frac{\omega^2}{gH}\left(\frac{B}{\delta_A\sinh(\delta_A)} - 1\right)^{-1}}, \tag{6}$$

in which $A_{v,ti}$ is the vertical eddy viscosity acting on the tidal flow. Note that we split subtidal horizontal velocity in a depth-averaged and a depth-dependent component, but do not make this separation for tidal velocity. Furthermore, $A_{v,ti}$ and therefore u_{ti} do not depend on salinity.

For salinity, no analytical expressions are obtained, but the decomposition from Eq. 2 is substituted in the 2DV mass balance for salinity, which reads

$$\frac{\partial s}{\partial t} + \frac{1}{b}\frac{\partial}{\partial x}(bus) + \frac{\partial}{\partial z}(ws) = \frac{1}{b}\frac{\partial}{\partial x}\left(bK_h\frac{\partial s}{\partial x}\right) + \frac{\partial}{\partial z}\left(K_v\frac{\partial s}{\partial z}\right). \tag{7}$$

Here, K_h is the horizontal dispersion coefficient and K_v is the vertical eddy diffusivity coefficient. To obtain an equation for subtidal, depth-averaged salinity $\bar{s}_{st}$, we average this equation over depth and the tidal timescale, which gives

$$\frac{\partial\bar{s}_{st}}{\partial t} + \bar{u}_{st}\frac{\partial\bar{s}_{st}}{\partial x} + \overline{u'_{st}\frac{\partial s'_{st}}{\partial x}} + \left(\overline{\bar{u}_{ti}\frac{\partial\bar{s}_{ti}}{\partial x}}\right)_{st} + \left(\overline{u'_{ti}\frac{\partial s'_{ti}}{\partial x}}\right)_{st} = \frac{1}{b}\frac{\partial}{\partial x}\left(bK_{h,st}\frac{\partial\bar{s}_{st}}{\partial x}\right). \tag{8}$$

In this expression, $K_{h,st}$ is the horizontal dispersion coefficient acting on the subtidal salinity. The equation for the vertically varying part of the subtidal salinity s'_{st}, obtained from subtracting Eq. 8 from the tidally averaged mass balance, reads

$$\frac{\partial s'_{st}}{\partial t} + \bar{u}_{st}\frac{\partial s'_{st}}{\partial x} + u'_{st}\frac{\partial \bar{s}_{st}}{\partial x} + u'_{st}\frac{\partial s'_{st}}{\partial x} - \overline{u'_{st}\frac{\partial s'_{st}}{\partial x}} + w_{st}\frac{\partial s'_{st}}{\partial z} + \left(\bar{u}_{ti}\frac{\partial s'_{ti}}{\partial x}\right)_{st} + \left(u'_{ti}\frac{\partial \bar{s}_{ti}}{\partial x}\right)_{st}$$

$$+ \left(u'_{ti}\frac{\partial s'_{ti}}{\partial x}\right)_{st} - \overline{\left(u'_{ti}\frac{\partial s'_{ti}}{\partial x}\right)_{st}} + \left(w_{ti}\frac{\partial s'_{ti}}{\partial z}\right)_{st} = \frac{1}{b}\frac{\partial}{\partial x}\left(bK_{h,st}\frac{\partial s'_{st}}{\partial x}\right) + \frac{\partial}{\partial z}\left(K_{v,st}\frac{\partial s'_{st}}{\partial z}\right). \quad (9)$$

Here, $K_{v,st}$ is the vertical eddy diffusivity coefficient, acting on the subtidal salinity. An equation for tidally varying salinity s_{ti} is obtained, by subtracting the tidally averaged mass balance from the full mass balance. Additionally, only the dominant tidal constituent is considered, i.e. $s_{ti} = \Re[\hat{s}_{ti}\exp(-i\omega t) + c.c.]$, and scaling analysis is applied to select the most important terms. The equation governing the dynamics of $\hat{s}_{ti}$ is

$$-i\omega\hat{s}_{ti} + \hat{u}_{ti}\frac{\partial \bar{s}_{st}}{\partial x} + \hat{w}_{ti}\frac{\partial s'_{st}}{\partial z} = \frac{\partial}{\partial z}\left(K_{v,ti}\frac{\partial \hat{s}_{ti}}{\partial z}\right), \quad (10)$$

in which $K_{v,ti}$ is the vertical eddy diffusivity coefficient, acting on the tidally varying salinity. This equation has an analytical solution, i.e. $\hat{s}_{ti}$ can be expressed as a function of s_{st}, but this expression is very lengthy and therefore not presented here. To numerically solve for $\bar{s}_{st}$ and s'_{st}, a Galerkin method is used in the vertical and central differences in the horizontal. For time integration, a backward Euler scheme is employed.

2.4 Salt transport

The horizontal salt transport T in the model (which follows from the decomposition of currents and salinity as in Eq. 2), integrated over the tidal cycle and cross-section, and after neglecting terms that contain η (see Biemond et al. (2024a)), reads

$$T = \underbrace{Q\bar{s}_{st}}_{T_Q} + \underbrace{bH\overline{u'_{st}s'_{st}}}_{T_E} + \underbrace{bH\overline{(u_{ti}s_{ti})}_{st}}_{T_T} - \underbrace{bHK_{h,st}\frac{\partial \bar{s}_{st}}{\partial x}}_{T_D}. \quad (11)$$

The component T_Q is the salt transport due to advection by the depth-averaged subtidal current, T_E is the salt transport by the exchange flow, T_T is the salt transport due to time correlation of tidal flow and salinity and T_D is the salt transport due to horizontal dispersion. In our model, unresolved upstream salt transport processes are parametrised by the last term. Note that T_T could be further decomposed into a contribution that involves only the depth-averaged tidal current and a contribution that is due to the departure of the tidal current from its depth-averaged value. The values of vertical eddy viscosity, vertical eddy diffusivity and horizontal dispersion coefficients are assumed to be constant throughout the entire domain. For bottom friction, a partial slip condition is applied at the bed, with friction coefficient $S_f = \frac{2A_v}{H}$, where A_v is the vertical eddy viscosity and H is the water depth. Note that the values of the coefficients used for eddy viscosity, eddy diffusivity, dispersion and friction depend on whether they act on the tidal or subtidal current and salinity, as is explained in e.g. Godin (1991, 1999).

2.5 Boundary conditions

Regarding the boundary conditions at river boundaries: subtidal discharge is prescribed, tides are assumed to dissipate in the river beyond the boundary (without reflection at a horizontal boundary), and subtidal salinity is set to the river salinity. Hence

$$bH\bar{u}_{st} = Q_{riv}, \quad C_1 = 0, \quad \bar{s}_{st} = s_{riv}, \quad s'_{st} = 0. \tag{12}$$

Here, Q_{riv} and s_{riv} are the river discharge and salinity, respectively, which are generally non-zero. The condition $C_1 = 0$ physically means that there is no downstream travelling tidal wave.

At weir boundaries we prescribe subtidal discharge and use a reflecting boundary condition for the tidal flow, such that the water transport vanishes at such boundaries. For salinity, we impose conditions on the salt transport. When the discharge at the weir is into the domain (which is usually the case), the depth-averaged transport equals a prescribed salinity s_{weir} multiplied with the discharge. When the discharge at the weir is out of the domain (which is e.g. the case for the Haringvliet sluices in the RMD), the depth-averaged transport is set to the calculated salinity at the weir multiplied with the discharge. The vertical variations of the dispersive salt flux are set to zero, to avoid formation of a dispersive boundary layer (Biemond et al., 2024b). In summary, the boundary conditions read

$$bH\bar{u}_{st} = Q_{weir}, \quad \int_{-H}^{0} u_{ti}dz = 0, \quad T = Q_{weir}s_{weir}, \quad K_{h,st}\frac{\partial s'_{st}}{\partial x} = 0, \tag{13}$$

in which Q_{weir} is the discharge at the weir, and s_{weir} is prescribed in the case of the discharge being from the weir and the local (depth-averaged) salinity in case of a discharge towards the weir.

Water levels η_{st} and η_{ti} are prescribed at sea boundaries (estuary mouths). To obtain conditions for salinity, additional segments are added that extend seaward from the mouths. These segments are characterised by strongly increasing widths away from the mouths. At the outer sea boundaries of these segments, salinity is set to the sea salinity. Furthermore, assuming that at these locations there is only an incoming tidal wave (i.e. travelling from sea to estuary) allows us to compute the water levels and tidal flow in these segments. The assumption made here is reasonable, because of the strongly increasing width of these segments.

At the junctions, continuity of discharge and water level is imposed. These conditions apply to the subtidal quantities as well as to the tidally varying quantities. Regarding salinity, continuity of salt transport and salinity is used at every vertical level. To apply conditions to the tidal salinity, a boundary layer correction is employed. At the boundaries between the channel segments, the same conditions are applied. The specific expressions for these boundary conditions are described in Appendix B and the boundary layer correction for tidal salinity is described in Appendix C.

2.6 Model implementation for the RMD

The implementation of the domain of the RMD in the model, as sketched in Fig. 2, consists of twenty-one channels, twelve junctions, one sea boundary, three weir boundaries, and two river boundaries. The channels consist of one or two segments.
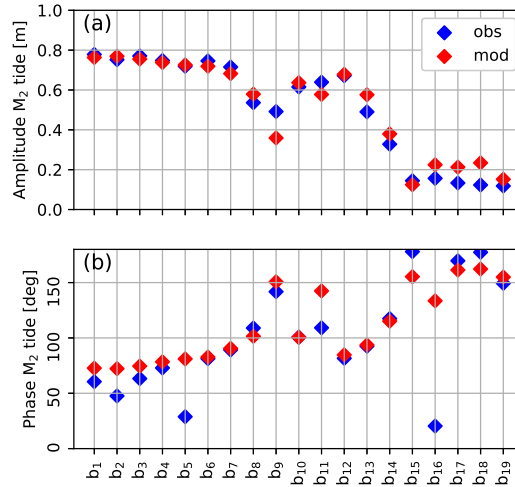
Figure 3. (a) Observed (in blue) and modelled (in red) amplitude of the M_2 water level for different points in the RMD, whose location is indicated in Fig. 1. (b) As (a), but for the tidal phase of the water level.

The division in multiple segments is based on the desired horizontal grid size and does not affect the physics. The Haringvliet sluices connect the Haringvliet channel with the open sea, and are only opened to release water from the Haringvliet, such that no salt intrudes through this boundary. The widths and depths of each channel are presented in Table A1. Note that a coarse representation of the geometry is used, so geometrical details (e.g. the harbour basins) are not resolved. In the following, we will refer to the different channels by their acronyms as specified in Fig. 2.

The horizontal grid size is around a few hundred meters, but differs per channel and is finer in regions where larger salinity gradients are expected. In the vertical, five Fourier modes are used for the Galerkin projection and the model time step (which only applies to subtidal quantities) is one day.

The model is forced with prescribed time series of discharge at the two river and the three weir boundaries, and with the water level amplitude and phase of the dominant tidal constituent, which is the semi-diurnal lunar M_2 tide (period 12 h, 25 m) for the RMD, at the North Sea boundary (note that the water level amplitude of the M_2 component at the station at the mouth (b_1) is four times larger than that of the second largest component (Walters, 1987)). For salinity, time-independent values are used, which are 0.15 g kg^{-1} at the river and weir boundaries and 33 g kg^{-1} at the North Sea boundary.

3 Results

3.1 Model-observation comparison

3.1.1 Method

To address the first aim (model-observation comparison), suitable values of eddy viscosity, eddy diffusivity and dispersion coefficients are needed. This is achieved by means of calibration: the modelled tidal water levels and salinities are compared with observed tidal water levels and salinities. There are nineteen water level stations in the RMD, indicated with b_1-b_{19} in Fig. 1, and seven salinity observation points, indicated with a_1-a_7 in this figure. At a number of these locations, salinity observations are available at two or three depths. There are only a few permanent current measurement stations available in the RMD and therefore currents are not evaluated. The discharge, water level and salinity data of the RMD are accessible at waterinfo.rws.nl. The year 2022 is used as calibration period, since this is a year with a low Rhine discharge, which is a situation in which salt intrusion is relevant. For the hydrodynamic module, the vertical eddy viscosity component acting on the tidal flow $A_{v,ti}$ is calibrated. An optimisation procedure is employed for this variable to find the minimum error between the modelled and the observed M_2 water level variations, using the skill score as used by Davies and Jones (1996), which computes a cost function f as

$$f = \sum_{k=1}^{N} \sqrt{(\hat{\eta}_k^{obs} - \hat{\eta}_k^{mod})^2 + 2\hat{\eta}_k^{obs}\hat{\eta}_k^{mod}\left(1 - \cos(\hat{\theta}_k^{obs} - \hat{\theta}_k^{mod})\right)}. \tag{14}$$

Here, N is the number of observations, $\hat{\eta}_k^{obs}$ and $\hat{\eta}_k^{mod}$ are the observed and modelled amplitude of the water level of the dominant tidal constituent, respectively, and $\hat{\theta}_k^{obs}$ and $\hat{\theta}_k^{mod}$ are the observed and modelled phases of the tidal water level, respectively.

Coefficients for subtidal vertical eddy viscosity $A_{v,st}$, subtidal vertical eddy diffusivity $K_{v,st}$, horizontal dispersion $K_{h,st}$ and tidal vertical eddy diffusivity $K_{v,ti}$ are calibrated by minimising the root-mean-squared error (RMSE) between observed and modelled time series of subtidal salinity at the observations points. A gradient descent algorithm is employed to find the optimal values of these parameters. After the calibration, the model performance regarding subtidal salinity is quantified by calculating the Nash-Sutcliffe efficiency (NSE) (Nash and Sutcliffe, 1970), which reads

$$NSE = 1 - \frac{\sum_{k=1}^{N}(s_k^{obs} - s_k^{mod})^2}{\sum_{k=1}^{N}(s_k^{obs} - <s_k^{obs}>)^2}, \tag{15}$$

where s_k^{obs} and s_k^{mod} are observed and modelled salinity, respectively, $< \cdot >$ indicates a time-averaged quantity. A score of $NSE = 1$ indicates perfect agreement, while $NSE = 0$ means that the model error is equal to the variance of the observed time series, and finally $NSE < 0$ indicates that the observed mean is a better predictor than the model.

3.1.2 Tides

The amplitudes and phases of the M_2 component of the water level in observations and the calibrated model are shown in Fig. 3. A minimum for f is obtained with $A_{v,ti} = 0.025$ m^{2}s^{-1}. The amplitude in the main channels is well resolved
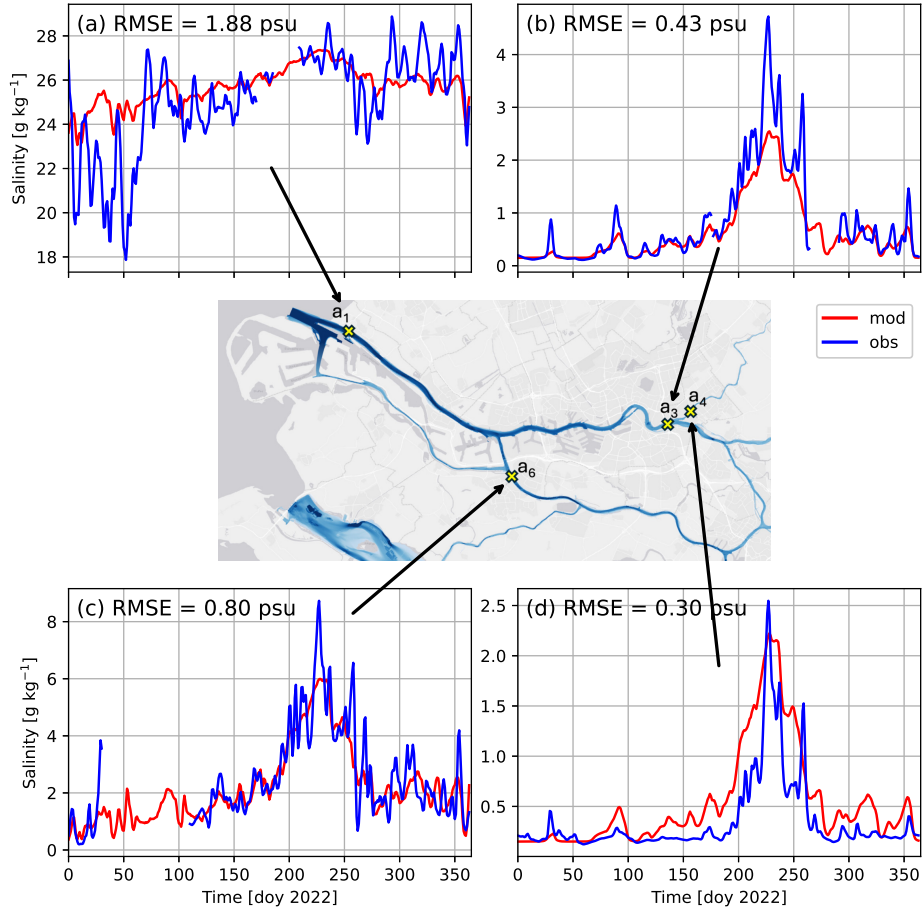
Figure 4. Observed (in blue) and modelled (in red) tidally averaged salinity time series for 2022 at four locations in the RMD: (a) a_1 ($z = -9.0$ m), (b) a_3 ($z = -2.5$ m), (c) a_6 ($z = -2.5$ m), and (d) a_4 ($z = -4.0$ m).

($b_1 - b_7$, $b_{12} - b_{14}$). In observation point b_9 (the LE channel), the amplitude is underestimated by 27%, and in the southern part ($b_{16} - b_{19}$), the amplitude is overestimated by 55% averaged over the four points. There are two outliers in terms of tidal phases (at points b_5 and b_{16}). The observed phase at point b_5 differs in such a way from the phase at the neighbouring points that probably an error in the raw data is responsible for the mismatch here. In point b_{16} the tides are affected by the operation of the Haringvliet sluices, which is not resolved in the model.

3.1.3 Salinity

The NSE (Eq. 15) for modelled and observed salinity after calibration is 0.67, which classifies the model performance as satisfactory (Moriasi et al., 2015). This result is found for $A_{v,st} = 0.0024$ m^{2}s^{-1}, one order of magnitude lower than the vertical eddy viscosity for tidal flow. Regarding vertical eddy diffusivities for tidal and subtidal salinity, the best agreement

is found when using $K_{v,st} = \frac{A_{v,st}}{Sc}$ and $K_{v,ti} = \frac{A_{v,ti}}{Sc}$, with $Sc = 2.2$, the Schmidt number. The horizontal subtidal dispersion coefficient $K_{h,st} = 275$ m^{2}s^{-1}, which is rather high compared to what was found for single-channel estuaries (Biemond et al.,
250 2024a). The reasons and implications of this will be discussed in Section 4.

Modelled and observed salinity in the RMD at four selected observation points is shown in Fig. 4. We refer to Fig. S1 for the comparison at the other observations points. Differences between the model and observations primarily concern an underestimation of the variability of the salt field. This is due to the fact that our model does not account for the spring-neap tidal cycle, overtides and subtidal and intratidal water level fluctuations at the sea boundary driven by remote winds, which have
255 a strong influence on the variability of the salinity. The model-data agreement is consistent at different depths for most stations where observations are available at multiple depths (Fig. S1), but the salinity in station a_1 is underestimated by 3.0 g kg^{-1} at $z = -9.0$ m averaged over first two months of the year, i.e. during high discharge conditions, while at $z = -2.5$ m no bias is present (compare Fig. S1b with Fig. S1d). This indicates that the relation between discharge and vertical salinity gradients in the model is not well resolved, which probably is due to the use of a constant vertical eddy viscosity and vertical eddy diffusivity.
260 In Fig. 4b, we see an underestimation of 0.6 g kg^{-1} averaged over the summer months, while in Fig. 4d, which is only a few kilometres from this location, the salinity is overestimated by 0.4 g kg^{-1} during this period. This probably originates from the large value of $K_{h,st}$, which reduces horizontal salinity gradients, but also the exclusion of other tidal constituents besides M$_2$ plays a role, as tidal flow is very important to salinity at point a_4, which will be shown in the next section.

3.2 Salt intrusion mechanisms

265 #### 3.2.1 Method

To quantify the mechanisms of salt transport in an estuarine network (the second research aim), an equilibrium simulation is performed with the calibrated model. To this end, the model is forced with discharges that represent low discharge conditions, as this is the situation in which salt intrusion is the most relevant. For the Haringvliet sluices, Hollandse IJssel and Lek rivers we set the discharge to zero, while for the Waal river we use $Q = 650$ m^{3}s^{-1} and for the Maas river $Q = 50$ m^{3}s^{-1}. These
270 values equal approximately the minimum observed discharges in the summer of 2022.

The distribution of net water transport and subtidal salinity in different channels in the RMD are presented in Fig. S2; the associated components of the salt transport in different channels in the RMD for low discharge conditions are shown in Fig. 5.

3.2.2 Main channels

It turns out that close to the sea boundary (BD, RW), salt transport related to the exchange flow T_E is the most important
275 contribution to the salt transport, while further inland its relative contribution decreases. This spatial pattern is explained by the fact that close to the sea boundary, depth is large, but further inland, the RMD becomes shallower (e.g. $H = 16$ m for BD and RW, but $H = 11$ m for NM1 and $H = 10.2$ m for OM3). The strength of the exchange flow u'_{st} scales with H^3 (Eq. 3c), and variable s'_{st}, which is mainly generated by this flow, thus decreases when depth decreases (Fig. S3). Salt transport component T_E is the product of those two and therefore strongly depends on depth.
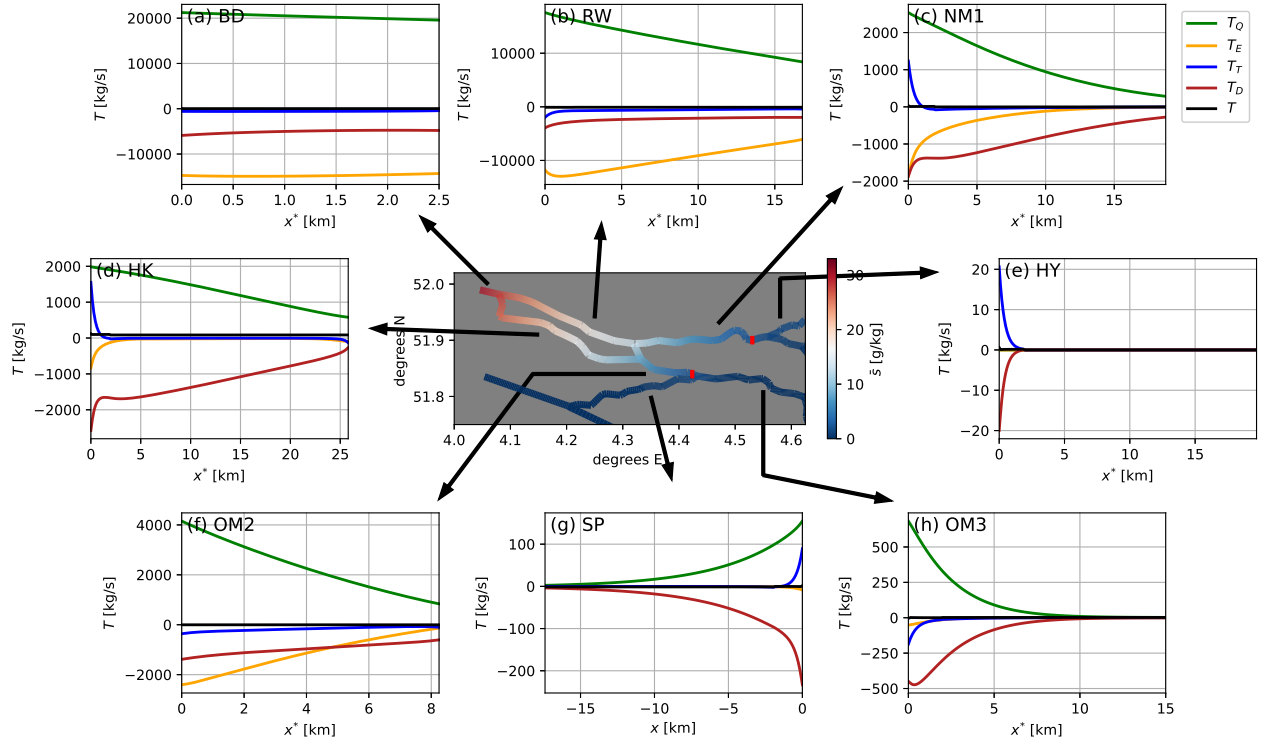
Figure 5. Center panel: depth- and tidally averaged salinity in the RMD for low discharge conditions. The red bars in this figure indicate the location of the 2 g kg^{-1} isohaline. (a)-(h) The different components of the salt transport in equilibrium, following the decomposition of Eq. 11, versus x or x^*, where we have defined $x^* \equiv -x$ for plotting purposes.

280 The salt transport component due to horizontal dispersion T_D becomes dominant in most areas where T_E declines (e.g. NM1, SP, OM3). This is because the dependence of T_D on depth is weaker (only through a decrease of the cross-section).

3.2.3 Tidal transport

The component due to tides T_T is small in most of the network. To explain this, we compute the phase difference between depth-averaged tidally varying flow and salinity, which is very important to the magnitude of T_T (see Eq. 11). A phase difference
285 of more (less) than 90 degrees is associated with an upstream (downstream) salt transport. In our model context, this phase difference is generated by two mechanisms: vertical advection of subtidal salinity within the tidal cycle (Biemond et al., 2024a), and interaction with other channels around junctions. The first mechanism requires the presence of tidally-averaged vertical salinity gradients, which mainly are created by the exchange flow. This gives, for example, a phase difference of about 95 degrees in the RW (Fig. S4), which yields $T_T \approx 500$ kg s^{-1}, about 15 times smaller than T_E. Note that a T_T of this strength
290 would be the dominant salt transport in channels further upstream, e.g. OM3. In the channels where exchange flow is weaker,
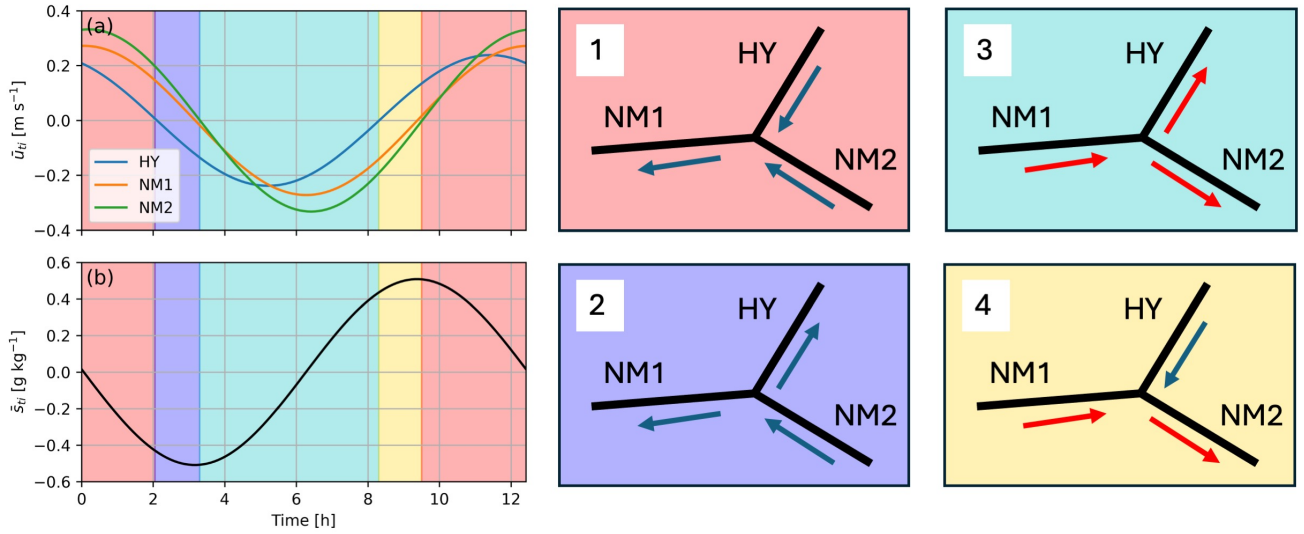
Figure 6. (a) Depth-averaged tidal velocity $\bar{u}_{ti}$ within a tidal cycle at the junction of the Hollandse IJssel (in blue), Nieuwe Maas 1 (in orange) and Nieuwe Maas 2 (in green). (b) As (a), but for depth-averaged tidal salinity $\bar{s}_{ti}$. Panels 1-4: Visualisation of situation during different phases of the tide. The background colors correspond to the colors of panel a-b. The arrows indicate the direction of the current and its color indicates whether the water is relatively fresh (blue) or relatively saline (red).

the induced phase difference is also smaller, and therefore T_T is a subdominant component of the salt transport, except around some junctions. The net salt transport due to vertical variations of the tidally varying flow and salinity is not considered for this explanation, because their contribution to salt transport is negligible, as explained in Biemond et al. (2024a).

3.2.4 Transport in the vicinity of junctions

295   Near junctions such as the SP-OM2-OM3 or the BD-RW-HK, the distortion of the phase difference from 90 degrees increases strongly, e.g. around the seaward boundary of the HK, NM1 and HY, where the minimum phase difference is about 60 degrees (Fig. S4). Here, T_T also reverses sign, i.e. it becomes seaward, along the salinity gradient. Note that for each junction in only one connected channel the phase difference is below 90 degrees. To illustrate this behaviour, we study the case of the junction of the HY, NM1 and NM2 in detail, but similar reasoning applies to the other junctions. Fig. 6 visualises tidal currents and

300   salinity around this junction. Fig. 6a shows that $\bar{u}_{ti}$ in the HY leads the currents in the other two channels by about 1.5 hours. The consequences for the salt transport are made clear by studying the different phases of the tide. When the currents in all channels are positive, i.e. the red shaded area and panel 1, relatively fresh water from upstream is transported downstream, and salinity at the junction decreases (Fig. 6b). At some point, the current in the HY will change direction before the currents in the other channels change direction (the blue shaded area and panel 2). In this phase, the HY will receive freshwater from

305   upstream, i.e. from the NM2. After about 1.5 hours, currents in the other channels will also change direction (the light blue

area and panel 3), and saline water from downstream is imported into the channels. However, when salinity at the junction reaches its maximum value, $\bar{u}_{ti}$ in the HY has changed direction (the yellow area and panel 4), and this salinity does not reach the HY. The tidally averaged transport T_T is upstream in the main channels (NM1 and NM2), while it is downstream in the side channel (HY).

3.2.5 Minor channels

The HY (and also the LE) is a special case in a sense that it does not receive discharge from upstream and therefore T_Q is everywhere zero in this channel. The absence of discharge, which is the main source of buoyancy, also implies that (tidally averaged) vertical salinity gradients are almost absent: the top-bottom salinity difference is 0.09 g kg^{-1} at 1 km from the junction in the HY. This implies that T_E is weak, i.e. $\frac{T_E}{T_D} = 5 \cdot 10^{-4}$ at this location.

A similar situation occurs in the HK, which is shallower than its neighbouring channels, therefore receives less discharge (71 m^{3}s^{-1}, about 9 times smaller than the RW) and consequently is less stratified and the channel-averaged contribution of T_E to the upstream salt transport in the HK is only 4% (Fig. 5d).

3.2.6 Overspill

The absolute value of the total salt transport $|T| = 80$ kg s^{-1} in the HK, OM1 and RW, indicating the presence of salt overspill in these channels. Overspill occurs when salt originating from one channel is transported downstream with the subtidal current $\bar{u}_{st}$ through another channel. In Fig. S2 the direction of this transport is indicated. For the range of values of the parameters investigated in this study, this only occurs in the RW-OM1-HK channel system in the RMD. Under the low discharge conditions studied here, its contribution to the total salt transport in the HK is 13%.

3.3 Response to changes in discharge

3.3.1 Method

To examine the response of salinity in the network to changes in discharge (the third research aim), the model is forced with discharge time series that represent the transition from reference discharge conditions to low discharge conditions and vice versa. For the Haringvliet sluices and the Hollandse IJssel river, discharge is set to zero. In the reference situation, the Lek, Waal and Maas rivers are forced with their long-yearly average discharge, which are 490, 1500 and 230 m^{3}s^{-1}, respectively. To simulate the response to a transition to low discharge conditions, the reference discharges are multiplied with a factor, ranging from 0.95 to 0.2 for the different scenarios. In this way, the fraction of the total discharge received per channel does not change. The simulation is continued until equilibrium has been reached. To simulate the response to an increase in river discharge, discharge is increased from the lowered value to the yearly average values, and again the simulation is continued until equilibrium has been obtained. Note that these simulations do not reproduce the current water distribution in the RMD during a drought, because discharge in the three rivers does not change with the same ratio, due to water management and
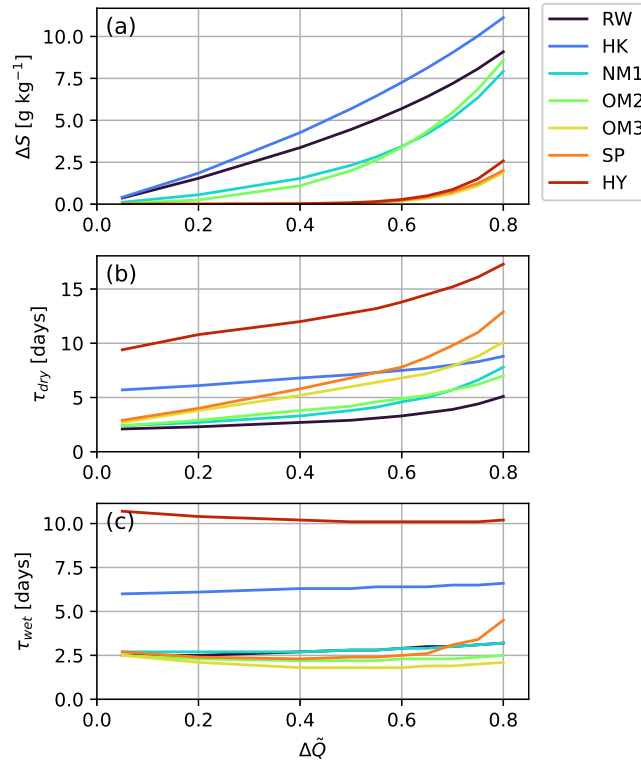
Figure 7. (a) Absolute value of the change in channel-averaged salinity ΔS of different channels as a function of change in discharge $\Delta \tilde{Q} = \frac{Q_{ref} - Q_{dry}}{Q_{ref}}$, where Q_{ref} is the yearly average discharge and Q_{dry} the decreased discharge. Note that ΔS is independent of the sign of the change in discharge, because absolute values are considered. (b) As (a), but for the response time τ_{dry} due to a decrease in river discharge, i.e. a transition from Q_{ref} to Q_{dry}. (c) As (b), but for the response time τ_{wet} due to an increase in river discharge, i.e. a transition from Q_{dry} to Q_{ref}.

local differences in drought intensity. Moreover, the Haringvliet sluices are opened when the discharge is high, closed for low discharge, and partially opened in between.

For quantification of the salinity response to a change in discharge, studies for single-channel estuaries have analysed the evolution of a certain isohaline, typically the 2 g kg^{-1} isohaline (Chen, 2015; Monismith, 2017). However, in a network this is

340   not generally possible, as isohalines are not bound to a certain channel. Therefore, an alternative measure for the salt intrusion in a channel is used for response times, which is based on the channel-averaged salinity S, defined as $S = \frac{\int_V s_{st} dV}{V}$, where V is the volume of the channel. The response time is then defined when 90% of the change in S has occurred (Note that S goes to a constant value after the change in discharge). We indicate the time it takes to respond to a low discharge with τ_{dry} and the time it takes to respond to a high (i.e. the reference) discharge with τ_{wet}.

3.3.2 General behaviour

The changes in mean salinity and the response times of individual channels in the RMD after an increase and decrease in discharge of the Lek, Waal and Maas rivers are shown in Fig. 7. A larger change in discharge is associated with a larger change in mean salinity, as expected. The absolute changes in salinity are larger for channels close to the sea (RW, HK), but smaller for channels close to the limit of the salt intrusion (SP, HY, OM3). Regarding response times, τ_{dry} increases for larger changes in discharge (τ_{dry} associated with an 80% change in discharge is 61% larger than τ_{dry} of a 5% change for the channels considered in Fig. 7), but τ_{wet} is not sensitive to the magnitude of the change in discharge (τ_{wet} associated with an 80% change in discharge is only 9% larger than τ_{wet} of a 5% change for the channels considered in Fig. 7). This implies that τ_{dry} and τ_{wet} differ little for small changes in discharge, but that τ_{dry} exceeds τ_{wet} for larger changes in discharge.

Following Biemond et al. (2022), who also found this result for single-channel estuaries, the explanation is that τ_{dry} equals change in salt content, which scales with the change in salinity, divided by salt import due to T_E and T_D, which depend on the salinity gradient during the adjustment. The change in salinity and salinity gradient are in another manner related to the change in discharge and therefore τ_{dry} depends on the change in discharge. On the other hand, τ_{wet} is mostly determined by the change in salt content divided by the export of salt due to T_Q, which both scale linearly with salinity and therefore their ratio does not depend on the change in discharge.

The channels closer to the estuary mouth, i.e. those with a high salinity (RW, NM1), have a smaller τ_{dry} than the channels with a low salinity (HY, SP). This is because channels with a higher salinity also have larger horizontal and vertical salinity gradients (Figs. S3 and S5), which increases the magnitude of the salt import by T_E and T_D.

3.3.3 Minor channels

The HK and HY have larger response times than their neighbouring channels. Focussing first on the HK, for which τ_{dry} is a factor two higher than in the RW, despite the salinity and salinity gradients being comparable. To explain this, we calculate the total change of salt content in this channel, which equals the channel volume V multiplied with the change in its average salinity ΔS, divided by its salt import in equilibrium at the downstream boundary $T_r = \frac{V\Delta S}{T_E+T_D+T_T}$, which is a lower bound of τ_{dry}. The salt exchange at the upstream boundary is a factor of six smaller in this channel (Fig. 5d) and therefore not taken into account here. We find $T_r = 18.4$ h for the HK and e.g. $T_r = 4.0$ h for the NM1 and $T_r = 3.0$ h for the OM2. Thus, the ratio between salt exchange with the neighbouring channels to the total change in salt content in the HK is smaller than for neighbouring channels, which is because this channel receives little discharge, and this explains the larger τ_{dry}. The same reasoning holds for the fact that τ_{wet} of this channel is larger than in its neighbours, as in equilibrium the salt import equals the salt export, and therefore the salt export is also relatively small.

3.3.4 Closed channels

In the HY, τ_{dry} is about a factor two higher than that of the other channels. In channels without net water transport like the HY, equilibrium with the forcing conditions will be reached when the horizontal salinity gradient is zero in the channel interior,

i.e. when the salinity at the upstream boundary equals the salinity just outside the boundary layer around the junction. This means that the salt front has to intrude over the full length of the channel, which makes that the response time is larger than for channels with net water transport. Moreover, only salt transport component T_D (see Section 3.2) imports salt in this channel during the adjustment process, while T_T exports salt around the junction (Fig. 5e). The high τ_{dry} of the HY, and more general of channels without discharge, is thus explained by the fact that salt import by T_E is absent and that salt has to intrude over the full length of the channel.

Fig. 7c shows that also τ_{wet} is high in the HY, because there is no discharge through the channel which flushes the salinity (through T_Q). Instead, salt is removed by T_D and T_T. Like for the other channels, τ_{wet} is smaller than τ_{dry} in the HY, but different mechanisms play a role here than for most other channels. First, T_T has the same sign as T_D in the boundary layer around the junction when salinity in the channel decreases, so salt export during a decrease in salinity is faster than salt import during an increase in salinity. Second, the salinity in the channels where it is connected to responds faster to an increase in discharge than to a decrease in discharge (compare τ_{wet} and τ_{dry} of NM1).

3.4 Response to changes in depth

3.4.1 Method

Effects of changes to the depth of individual channels on salt intrusion in the major branches (the fourth research aim) are quantified from analysing output of a set of equilibrium simulations that have the same forcing conditions as the simulation for the second research aim. In each of these simulations, the depth of one of the channels in the network is increased or decreased by 25%. The impact on the salt intrusion is quantified by means of the distance X_2 from the RW-NM1-OM1 junction to the subtidal 2 g kg^{-1} isohaline in the Nieuwe Maas (consisting of channels NM1 and NM2) and in the Oude Maas (consisting of channels OM1, OM2, OM3, OM4), the two major branches of the network. The locations of these isohalines are shown in the centre panel of Fig. 5. These quantities can be converted into distance to the sea boundary by adding the length of the BD and that of RW, which is 19.3 km in total.

Salt intrusion lengths X_2 of the Oude Maas and Nieuwe Maas for changes to the depth of individual channels are shown in Fig. 8a. In contrast to the simulations for Section 3.3, the net water transport distribution changes when the depth changes, and the values for the major branches are presented in Fig. 8b. The responses of the salt intrusion lengths range from no detectable change in X_2 to a maximum change of 12 km. In the following, we will explain the mechanisms that are responsible for the different responses.

3.4.2 Seaward channels

Changes in depth of the most seaward channels (BD and RW) affect the extent of the salt intrusion (increases when deepening, decreases when shoaling), because upstream salt transport in these channels is dominated by T_E (Fig. 5a), which depends strongly on the local depth (Section 3.2). Changing the depth of the RW has a larger effect on X_2 than changing the depth of the BD because the RW is longer.
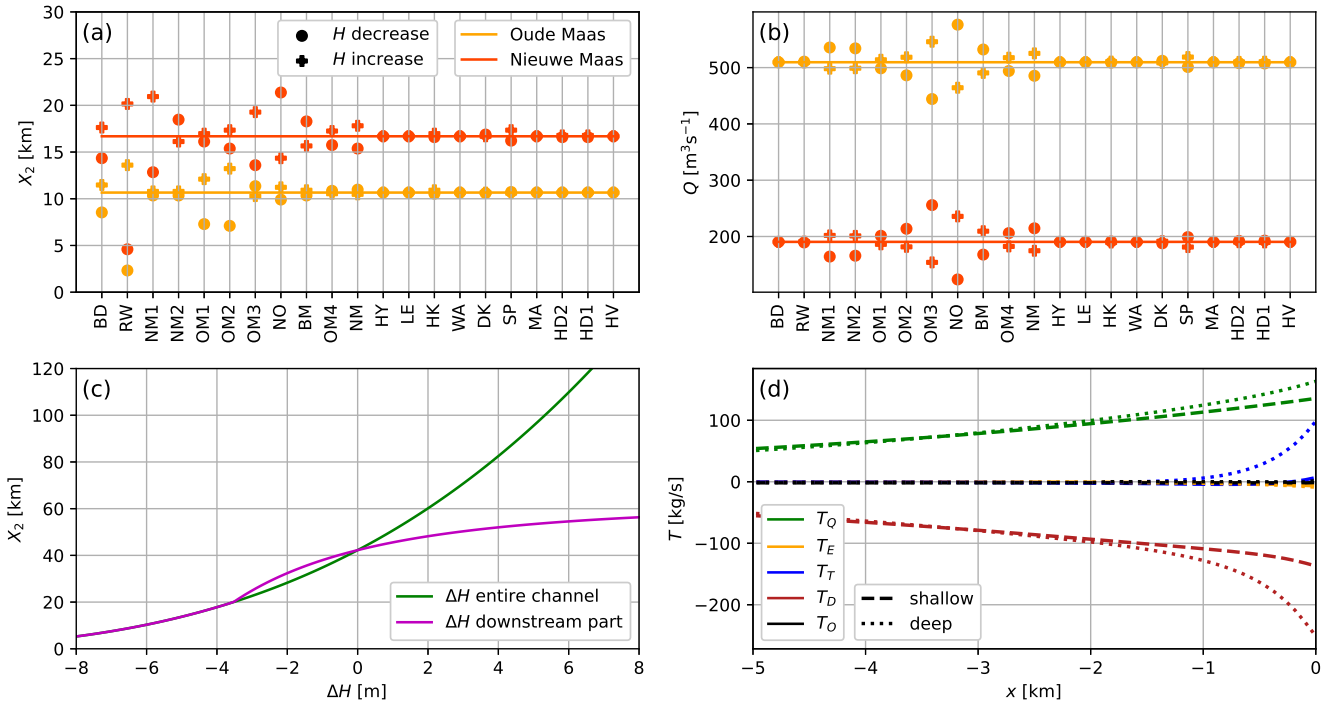
Figure 8. (a) The salt intrusion length X_2, defined as distance from the RW-NM1-OM1 junction to the 2 g kg^{-1} isohaline in the Oude Maas (yellow), Nieuwe Maas (red), versus changes in depth of different channels. The dots indicate a decrease in depth, and the plus markers indicate an increase in depth. The lines indicate X_2 with the current geometry. (b) As (a), but for the net water transport through OM1 (yellow) and NM1 (red). (c) Salt intrusion length X_2 of a single-channel estuary that consists of two segments, as a function of change in depth ΔH of the entire estuary (green) or change in depth of the downstream 20 km (purple), around a reference depth of 16 m (the depth of the RW), using Eqs. D4 and D5. (d) As Fig. 5g, but for a shallowed HD1 (dashed line) or a deepened HD1 (dotted line) and zoomed in on the 5 km of the channel adjacent to the SP-OM2-OM3 junction.

The magnitude of the change in X_2 due to a decrease $+\Delta H$ in depth exceeds the change after an increase $-\Delta H$. Scaling relations between depth and extent of the salt intrusion in single-channel estuaries (Monismith et al., 2002) predict a scaling with H^3 when T_E is the dominant salt import mechanism, which implies that, in contrast with what we find, an increase in depth would result in a larger absolute change in X_2 rather than a decrease.

To understand why the scaling is different in a network, a simple model for the RW is constructed, which mimics the RW as a single-channel estuary, but with two segments, and assumes a balance between T_Q and T_E (the Chatwin (1976) balance), which are the dominant salt transport components in the RW (Fig. 5b). The details of the model are in Appendix D. In this case, analytical solutions for the salt intrusion length as a function of depth are obtained. Two scenarios are considered: in the first, the depth of the entire channel is changed. In the second, only the depth of the downstream 20 km long segment of the channel is changed. The results are shown in Fig. 8c. When the depth of the entire channel is changed (the green line), an increase in

depth has a larger impact than a decrease in depth, which follows from the earlier mentioned H^3 scaling (Eq. D2). However, when the depth of only the downstream part of the channel is changed (the purple line), a deepening $+\Delta H$ has a smaller effect than shoaling $-\Delta H$. This is because when the depth is increased, salt intrusion length increases, and only a limited part of the salt intrusion experiences a larger depth and the associated increase in salt transport. In case of shoaling, the salt intrusion length decreases and a relatively large part of the salt intrusion experiences a smaller depth and the related decrease in salt transport. As the RW and BD are within the range of salt intrusion, increasing their depth has a smaller effect than decreasing their depth.

3.4.3 Main channels

For changes to the depth of channels which are part of major branches Oude Maas and Nieuwe Maas, two competing mechanisms play a role. The first is that deepening increases the magnitude of T_E. The second mechanism is that, simultaneously, the net water transport through the branch will increase, due to a decrease in friction, causing an increase in T_Q. Because of volume conservation, the magnitude of the change in net water transport is equal for the other major branch, but with an opposite sign. The change in friction when changing the depth also affects the tidal currents, but the changes in salt transport component T_T are negligible. The interplay of these mechanisms makes that when deepening channels that are part of the major branches and within the limit of the salt intrusion, i.e. the NM1, OM1, and OM2, salt intrusion increases. This is because locally the magnitude of T_E increases, which dominates over the increase in T_Q. In the other major branch, salt intrusion increases as well, because net water transport decreases (Fig. 8b). On the other hand, changing the depth of channels that are part of the major branches but outside the limit of the salt intrusion (NM2, OM3) does not affect T_E directly, but only T_Q. This makes that an increase in depth decreases salt intrusion in the major branch where the channel is part of, and simultaneously increases salt intrusion in the other major branch. Note that the statements in this section are given for deepening. For shoaling, we find the opposite effect. Changes in net water transport also explain the response of channels that are important for the distribution of the Waal river discharge, i.e. the NO, BM, OM4 and NM. Especially the NO has a large effect on salt intrusion in the Nieuwe Maas, as this channel exerts a strong control on the amount of discharge from the Waal river that reaches the Nieuwe Maas. The salt intrusion in the Nieuwe Maas is more sensitive to changes in net water transport than the Oude Maas, because the net water transport through the Nieuwe Maas is about 2.5 times smaller than that of the Oude Maas (Fig. S2).

3.4.4 Other channels

Changes in the depth of the other channels in the RMD (in Fig. 8a HY and all to its right) have little impact on X_2 in the Nieuwe Maas and Oude Maas (changes are less than 1 km). There are however two cases, that have an interesting local effect. The first concerns a change of depth in the HK. In the reference simulation, salt overspill occurs in the HK ($T = 80 \; \mathrm{kg \, s^{-1}}$) and salt from the Oude Maas is transported seawards through the HK (Figs. 5d and S2). When decreasing its depth, the magnitude of the salt transport due to salt overspill increases ($T = 540 \; \mathrm{kg \, s^{-1}}$), but when increasing the depth, the sign of T reverses and the HK becomes a source of salt for the Oude Maas ($T = -250 \; \mathrm{kg \, s^{-1}}$). The consequence of this change in salt transport for the salt intrusion length is only a few hundred meters, because this salt transport is relatively weak compared to the amount of

salt transported from the RW into the Oude Maas. The second interesting behaviour concerns an increase or decrease of the depth of the HD1. These have little impact on X_2 in the Oude Maas and Nieuwe Maas, but affect the extent of the salt intrusion into the SP. The distance of the 0.5 g kg^{-1} isohaline in the SP to the junction with the OM2 and OM3 is 6.3, 5.2 and 4.8 km for the shallow, reference and deep HD1, respectively, so shoaling the HD1 affects salt intrusion more than deepening. To understand this, we calculate the change in salt transport components T_Q and T_T (the flow associated with these components of the salt transport directly changes in the SP due to a change of the depth of the HD1). The difference in T_Q is about 30 kg s^{-1} between the shallow and deep HD1. Fig. 5g shows that for the reference depth T_T in the SP close to its seaward boundary is positive, in other words, salt transport due to tidal currents is directed towards the SP-OM2-OM3 junction. Fig. 8d shows that this situation persists for a deep HD1, but when decreasing the depth of HD1, the magnitude of T_T decreases, due to a shift in phases of the tidal currents of the different channels around this junction. The difference in T_T at the junction is about 90 kg s^{-1}, three times larger than the change in T_Q, indicating that the change in tidal currents dominates the change in salt intrusion into the SP when deepening the HD1.

4 Discussion

4.1 Comparison with observations

When our idealised network model is applied to the RMD and calibrated against observations, it has a Nash-Sutcliffe efficiency of 0.67. This indicates that the model performance with regard to simulating salinity is satisfactory, despite the fact that the descriptions of the physics, forcing conditions and bathymetry are rather simple. The gradient descent algorithm to find optimal values of the calibration coefficients is crucial to obtain a satisfactory model performance.

The effects of the non-resolved aspects of the salinity dynamics on the salt transport are via the calibration mostly projected on horizontal salt dispersion. A value of $K_{h,st} = 275$ m^{2}s^{-1} is found, and with this value T_D, the tidal dispersion, is the dominant salt transport component in parts of the RMD, in particular around the limit of the salt intrusion. However, since most of the observations points are in the larger channels of the network, this value of tidal dispersion mainly represents the unresolved salt transport in these channels. A hint that in the smaller channels of the network this constant value is too large follows from the described difference in model-data agreement between point a$_3$ and a$_4$ (see Section 3.1). Model extensions which could possibly resolve this disagreement are discussed in Section 4.4.

4.2 Changes in discharge

We found that response times vary between the channels and attributed this to differences in the salinity gradients, volume/-transport ratios of the channels, and the presence of net water transport in the channels. Observations show that response times to changes in forcing are observed to be 10-14 days for the HY (Laan et al., 2021), in line with what we find. In another estuarine network, the Po Delta, differences in response times between the channels are minor (Bellafiore et al. (2021) Fig. 5a). This is because in that delta all channels receive a considerable fraction of the river discharge and differences in channel depth are

also relatively small compared to the RMD. Therefore, dynamics of e.g. side branches, like the HY in the RMD, do not play a role in the Po Delta. Certain aspects of the theory of response of single-channel estuaries to changes in river discharge can be transferred to estuarine networks, e.g. the reason for the asymmetry in the response to an increase or decrease in discharge. However, a direct comparison with single-channel estuaries is hindered by e.g. differences in definitions of response times for reasons that were explained in Section 3.3.

4.3 Changes in depth

We showed that in a network, the response of the salt intrusion to changes in depth is sensitive to which channel is changed. Salt intrusion can decrease locally when parts of an estuarine network are deepened, due to a redistribution of the river water. This is different for single-channel estuaries, for which it is found that salt intrusion increases when the depth increases (Ralston and Geyer, 2019; Siles-Ajamil et al., 2019; Kolb et al., 2022). Liu et al. (2019) also reported effects on salt intrusion when upstream in a network (the Pearl River Delta) discharge changes due to alterations of the depth. For the Yangtze Estuary, Zhu et al. (2006) reported that salt intrusion increased in multiple channels when the depth of one the channels was increased, in line with what we find for the RMD. Huismans and Plieger (2019) showed, using a 3D model of the RMD, that a shallower Oude Maas leads to a decrease of salt intrusion in the Nieuwe Maas as well as in the Oude Maas. However, when winds and storm surges are accounted for, a more complicated response to changes in depth occurs. They hypothesised that changes in phases of the currents around the junction could be important to the response to changes in depth; we showed that they indeed can play an important role. For a deepening of the RW, Laan et al. (2023) found that salt intrusion in the entire RMD changes, but when deepening the LE, the effect remains local, which is again in line with what we find.

4.4 Future research

As explained in Section 2.1, certain model aspects are highly simplified, which limits the range of simulated salt dynamics in estuarine networks. The fact that only one tidal constituent is considered and that the balances for tidal flow and salinity are simplified implies that not all processes contributing to salt transport by the tidal current are included. Also, the vertical eddy viscosity, vertical eddy diffusivity and horizontal dispersion coefficients are assumed to be constant in space and time in our model. Considering these coefficients to vary with bathymetry, would lead to a different response to changes in bathymetry.

We present here recommendations on how to improve these model aspects, to gain more insight in the salt dynamics in estuarine networks. To improve the description of tidal salt transport, additional mechanisms which generate a phase difference between tidal currents and salinity, e.g. multiple tidal constituents (externally forced and internally generated), lateral effects (Scully and Geyer, 2012) or tidal trapping in side embayments (Okubo, 1973; Geyer and Signell, 1992; MacVean and Stacey, 2011) could be included. However, to find a suitable description of these processes in the simplified model may not be straightforward. Next, more realistic parametrisations of vertical eddy viscosity, vertical eddy diffusivity and horizontal dispersion coefficients could be employed. Other studies argue that the vertical eddy viscosity and vertical eddy diffusivity coefficients increase with strength of the tidal currents and with increasing depth of channels, and decrease with increasing stratification (Monismith et al., 2002; MacCready, 2007). These effects could be included to improve the description of the

turbulence closure of the model. For the horizontal dispersion coefficient, different parametrisations are proposed (Banas et al., 2004; MacCready, 2007; Aristizábal and Chant, 2015). However, the use of these formulations in our model is hindered by the fact that we resolve part of the salt transport by the tidal current explicitly.

Another direction for future research is the inclusion of additional forcing conditions, e.g. water level fluctations at subtidal and intratidal time scales at the sea boundary (Kranenburg et al., 2022), and water extractions, which are of order 100 m^{3}s^{-1} (Huismans et al., 2024), about one seventh of the total discharge in dry conditions.

5   Conclusions

The main findings, based on simulations with our idealised, partly analytical, 2DV model of an estuarine network, are the following:

1. The network model, when calibrated, has a satisfactory agreement with observations, despite missing potentially important aspects of the salinity dynamics. The reason for this is that the salt transport associated with these aspects projects well on the calibrated processes, especially on the horizontal salt dispersion. A consequence is that local variations in the salt transport due to tidal currents are only crudely resolved.

2. Salt transport components related to different mechanisms vary in relative importance within a network, due to differences in water depth, discharge, phases of the tidal currents and characteristics of the salt field itself. In the deeper channels of the RMD, upstream salt transport by exchange flow is dominant, but in the shallower parts tidal dispersion takes over. Salt transport by tidal currents can be directed seawards around a junction when the currents of the different channels are out of phase.

3. Channels closer to the estuary mouth respond faster to changes in discharge than those further upstream. The response to an increase in discharge is faster than the response to a decrease, in agreement with theory of single-channel estuaries. Channels which receive little discharge have large response times, especially when the net water transport is zero.

4. The impact of changes to the depth of an individual channel in a network on the extent of salt intrusion in the major branches depends on where the change takes place. The impact is determined by the direct, local effect on e.g. the strength of the exchange flow, and the interaction with other channels, which is related to changes in the distribution of discharge and tidal currents. Scaling relationships developed for single-channel estuaries are found to be invalid for depth changes in an estuarine network. Salt intrusion in a channel with lower discharge is more sensitive to changes in depth than a channel with higher discharge. The phase differences of tidal currents around a junction are sensitive to changes to the depth and this sensitivity can be the cause of changes in salt intrusion when the depth of a channel in another part of the network is changed.

545   *Code and data availability.* Software used in this study is made available online (Biemond, 2024). More recent versions of the model, called IMSIDE (Idealised Model of Salt Intrusion in Deltas and Estuaries), are available at https://github.com/nietBouke/IMSIDE. Used observational data can be downloaded from waterinfo.rws.nl.

Appendix A: Geometry of the Rhine-Meuse Delta

Table A1. Geometry of the Rhine-Meuse Delta used in the model. The abbreviations correspond to Fig. 2. The width at the boundaries of the channels are provided here, the width in the interior is computed with Eq. 1.

Channel	Abbreviation	Depth [m]	Length [km]	Initial width [m]	Final width [m]
Beneden Merwede	BM	6	15.3	100	300
Breeddiep	BD	16	2.5	1200	1200
Dordtsche Kil	DK	10.7	9.4	300	300
Haringvliet	HV	8.7	11.7	2420	2420
Hartelkanaal	HK	7.6	25.8	310	1500
Hollands Diep 1	HD1	7.6	32.0	1630	2000
Hollands Diep 2	HD2	6.2	3.81	1600	1100
Hollandse IJssel	HY	4.0	19.7	45	150
Lek	LE	5.3	42.0	136	260
Maas	MA	5.3	62.3	97	416
Nieuwe Maas 1	NM1	11	18.75	400	500
Nieuwe Maas 2	NM2	8.1	4.9	250	400
Nieuwe Merwede	NM	5	19.6	400	730
Nieuwe Waterweg	RW	16	16.8	600	600
Noord	NO	7	8.6	250	220
Oude Maas 1	OM1	13	3.1	250	250
Oude Maas 2	OM2	14	8.25	317	317
Oude Maas 3	OM3	10.2	15	240	350
Oude Maas 4	OM4	7	4.26	250	250
Spui	SP	6.4	17.4	250	250
Waal	WA	4	45.2	214	500

Appendix B: Conditions at internal boundaries

There are two types of internal boundaries in the model: connections between segments and junctions. The conditions below are given for junctions. For connections between segments the same conditions apply, but only two channels are considered. The conditions for hydrodynamics at the internal boundaries read

$$\sum_{p=1}^{3} b_p H_p \bar{u}_{st,p} = 0, \quad \eta_{st,1} = \eta_{st,2} = \eta_{st,3}, \quad \sum_{p=1}^{3} b_p H_p \bar{u}_{ti,p} = 0, \quad \eta_{ti,1} = \eta_{ti,2} = \eta_{ti,3}, \tag{B1}$$

where subscripts 1, 2 and 3 are indices of the channels which are connected to the junction. Regarding salinity, continuity of salt transport and salinity is used at every vertical level, which reads

$$\sum_{p=1}^{3} T_p = 0, \quad \bar{s}_{st,1} = \bar{s}_{st,2} = \bar{s}_{st,3}, \tag{B2a}$$

$$\sum_{p=1}^{3} b_p H_p \left(u'_{st,p} s'_{st,p} - \overline{u'_{st,p} s'_{st,p}} + (u'_{ti,p} s'_{ti,p} - \overline{u'_{ti,p} s'_{ti,p}})_{st} - K_{h,st} \frac{\partial s'_{st,p}}{\partial x} \right) = 0, \quad s'_{st,1} = s'_{st,2} = s'_{st,3}, \tag{B2b}$$

$$\sum_{p=1}^{3} b_p H_p \left(u_{ti,p} s_{ti,p} + u_{ti,p} s_{ti,p} - K_{h,ti} \frac{\partial s_{ti,p}}{\partial x} \right) = 0, \quad s_{ti,1} = s_{ti,2} = s_{ti,3}. \tag{B2c}$$

Note that the conditions for the vertically varying quantities are evaluated at sigma levels, i.e. at $\tilde{z} = \frac{z}{H} = $ constant, when the channels have a non-equal depth.

Appendix C: Boundary layer correction for salinity at junctions

The first-order equation for tidally varying salinity s_{ti} reads (Biemond et al., 2024a)

$$\frac{\partial s_{ti}}{\partial t} + u_{ti} \frac{\partial \bar{s}_{st}}{\partial x} + w_{ti} \frac{\partial s'_{st}}{\partial z} = \frac{\partial}{\partial x} (K_{h,ti} \frac{\partial s_{ti}}{\partial x}) + \frac{\partial}{\partial z} (K_{v,ti} \frac{\partial s_{ti}}{\partial z}), \tag{C1}$$

in which t is time, u_{ti} and w_{ti} are the horizontal and vertical component of the tidal current, respectively, $\bar{s}_{st}$ is the depth and tidally averaged salinity, s'_{st} is the vertical distortion from the tidally-averaged salinity and $K_{h,ti}$ and $K_{v,ti}$ are the horizontal dispersion coefficient and vertical eddy diffusivity coefficient, respectively, acting on the tidal salinity. The boundary conditions are no flux at the bottom and surface, and condition Eq. B2c for the horizontal boundaries (junctions). The horizontal dispersion term is included in Eq. C1. In Wei et al. (2016) and Biemond et al. (2024a) it was argued that this term is small with respect to the other terms in this equation. We argue here that horizontal dispersion is important in the neighbourhood of junctions, as tidal currents are observed to be more turbulent close to junctions (Corlett and Geyer, 2020), which increases the magnitude of dispersion. Moreover, when horizontal dispersion is excluded, Eq. C1 does not contain horizontal derivatives to s_{ti}, which implies that no horizontal boundary conditions can be applied, and therefore continuity of salinity at the junctions can not be imposed.

To develop a set of equations which takes horizontal dispersion into account around the junctions, we scale Eq. C1 by defining

$$t = \omega^{-1}\tilde{t}, \ x = L\tilde{x}, \ z = H\tilde{z}, \ u_{ti} = U\tilde{u}_{ti}, \ w_{ti} = H\omega \ \tilde{w}_{ti}, \ s_{st} = S_{st}\tilde{s}_{st}, \ s_{ti} = \frac{US_{st}}{\omega L}\tilde{s}_{ti}. \tag{C2}$$

In these expressions, ω is the frequency of the tide, L the horizontal length scale on which s_{ti} varies (when not being affected by junctions), U the magnitude of the tidal current, and S_{st} is a typical scale for the subtidal salinity. The last condition follows from $\frac{\partial s_{ti}}{\partial t} \approx u_{ti}\frac{\partial s_{st}}{\partial x}$ (Biemond et al., 2024a). This yields, after dropping the tildes,

$$\frac{\partial s_{ti}}{\partial t} + u_{ti}\frac{\partial \bar{s}_{st}}{\partial x} + \chi_1 w_{ti}\frac{\partial s'_{st}}{\partial z} = \varepsilon\frac{\partial^2 s_{ti}}{\partial x^2} + \chi_2\frac{\partial^2 s_{ti}}{\partial z^2}, \tag{C3}$$

with $\chi_1 = \frac{L\omega}{U}$, $\chi_2 = \frac{K_v}{\omega H^2}$ and $\varepsilon = \frac{K_h}{\omega L^2}$. We write tidally varying salinity as $s_{ti} = \Re[\hat{s}_{ti}\exp(-i\omega t) + c.c.]$ (see Section 2.3) and find the equation

$$\chi_2\frac{\partial^2 \hat{s}_{ti}}{\partial z^2} + i\hat{s}_{ti} + \varepsilon\frac{\partial^2 \hat{s}_{ti}}{\partial x^2} = \hat{u}_{ti}\frac{\partial \bar{s}_{st}}{\partial x} + \chi_1\hat{w}_{ti}\frac{\partial s'_{st}}{\partial z}. \tag{C4}$$

When choosing typical scales for an estuary ($H = 10$ m, $L = 10$ km, $U = 1$ m s^{-1}, $K_{h,ti} = 25$ m s^{-2}, $K_{v,ti} = 0.01$ m s^{-2} and $\omega = 1.4\cdot10^{-4}$ s^{-1}), it is found that χ_1 and χ_2 are of order one and ε is a factor 10^3 smaller. This defines a singular perturbation problem, which is solved using standard techniques (see e.g. Eckhaus (2011)).

To construct the regular solution, we write

$$\hat{s}_{ti,reg} = \sum_{n=0}^{\infty} \varepsilon^n \phi_n. \tag{C5}$$

Inserting this in Eq. C4 and collecting the first order terms gives Eq. 10, as expected, which is valid outside the neighbourhood of the junctions. Close to the junctions, we look for a correction to this equation, resulting from the horizontal dispersion. We write $\psi = \hat{s}_{ti} - \hat{s}_{ti,reg}$, and substitute this, which yields

$$\chi_2\frac{\partial^2 \psi}{\partial z^2} + i\psi + \varepsilon\frac{\partial^2 \psi}{\partial x^2} = -\chi_2\frac{\partial^2 \hat{s}_{ti,reg}}{\partial z^2} - i\hat{s}_{ti,reg} - \varepsilon\frac{\partial^2 \hat{s}_{ti,reg}}{\partial x^2} + u_{ti}\frac{\partial \bar{s}_{st}}{\partial x} + \chi_1 w_{ti}\frac{\partial s'_{st}}{\partial z}. \tag{C6}$$

We perform an expansion for the perturbation, i.e. $\psi = \sum_{n=0}^{\infty} \varepsilon^n \psi_n$. The first order solution then reads

$$\chi_2\frac{\partial^2 \psi_0}{\partial z^2} + i\psi_0 + \varepsilon\frac{\partial^2 \psi_0}{\partial x^2} = 0. \tag{C7}$$

Now a boundary layer coordinate ζ is introduced, i.e. we write $\psi_0 = B(z)e^\zeta$, with $\zeta = \pm\frac{x}{\varepsilon^\nu}$. It follows that $\nu = \frac{1}{2}$ when the horizontal dispersion term is of equal magnitude as the other terms in Eq. C7. Substitution of this gives the following equation for $B(z)$:

$$\chi_2\frac{d^2 B}{dz^2} + iB + B = 0. \tag{C8}$$

The no-flux boundary conditions at the bottom and surface apply to this equation. This is a homogenous problem, which has solution

$$B(z) = \sum_{m=0}^{\infty} B_m \cos\left(m\pi\frac{z}{H}\right). \tag{C9}$$

The values of B_m follow from the horizontal boundary conditions associated with the junction (Eq. B2c). With this, we have a solution for tidally varying salinity in the neighbourhood of the junctions (the extent of this region is determined by $\varepsilon^{\frac{1}{2}}$), which accounts for increased dispersion around the junctions and obeys the horizontal boundary conditions. We set $K_{h,ti} = 25 \, \text{m}^2\text{s}^{-1}$; sensitivity tests indicate that the model skill is insensitive to this value.

Appendix D: Derivation of the dependence of salt intrusion on the sign of the change in depth

To explain why an increase in depth of the Rotterdam Waterway (RW) has a smaller effect on salt intrusion in the Nieuwe and Oude Maas than a decrease, we develop a set of equations to study the difference between changing the depth of the downstream part of a channel versus the depth of the entire channel.
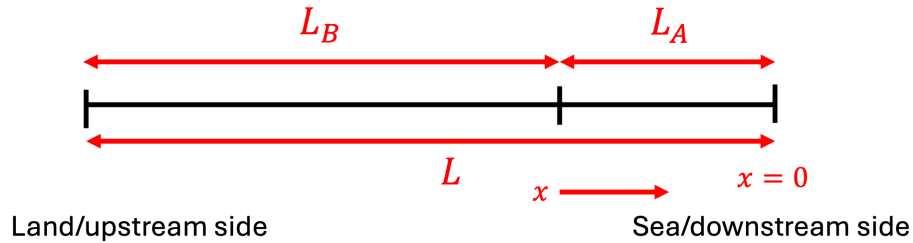
Figure D1. A sketch of the domain used in Appendix D.

Suppose we have a single-channel estuary with constant width in equilibrium, where the salt import is governed by exchange flow, like in the RW. In that case, the terms T_Q and T_E in Eq. 11 make balance with each other. If we furthermore assume that stratification is the result of a balance between advection of $\bar{s}_{st}$ by the depth-dependent part of the subtidal current and vertical eddy diffusion (Pritchard, 1954), the following equation for depth-averaged subtidal salinity $\bar{s}_{st}$ holds (Chatwin, 1976):

$$\frac{Q}{bH}\bar{s}_{st} = \frac{0.112}{48^2}\frac{g^2\beta^2 H^8}{A_{v,st}^2 K_{v,st}}\left(\frac{\partial\bar{s}_{st}}{\partial x}\right)^3. \tag{D1}$$

The domain is shown in Fig. D1 and the associated boundary condition is $\bar{s}_{st} = s_{oc}$ at $x = 0$.

In a single-channel estuary with length L and constant width, this equation has an analytical solution for salinity, which reads

$$\bar{s}_{st} = s_{sc}\left(\left(\frac{s_{oc}}{s_{sc}}\right)^{\frac{2}{3}} + \frac{2}{3}\frac{x}{L_e}\right)^{\frac{3}{2}} \quad \text{with} \quad L_e = \left(\frac{0.112}{48^2}\frac{bH}{Q}\frac{g^2\beta^2 s_{sc}^2 H^8}{A_{v,st}^2 K_{v,st}}\right)^{\frac{1}{3}}, \tag{D2}$$

where we have introduced salinity scale s_{sc}. To be able to change the depth of the downstream part of the channel separately, the single-channel estuary is divided in two segments with lengths L_A and L_B (see Fig. D1). In these segments, Eq. D2 with $L_e \to L_{e,A}$, the value of L_e in domain A, is valid for segment A, and for segment B we have

$$\bar{s}_{st} = s_{sc}\left(\left(\frac{s_{oc}}{s_{sc}}\right)^{\frac{2}{3}} - \frac{2}{3}\frac{L_A}{L_{e,A}} + \frac{2}{3}\frac{(x+L_A)}{L_{e,B}}\right)^{\frac{3}{2}}, \tag{D3}$$

where we have used continuity of salinity at the segment boundary (see Eq. B2a). Note that the values for $L_{e,A}$ and $L_{e,B}$ are different when the depths of the segments differ. From these expressions, we can find the position of a certain isohaline X_2 where salinity equals $s_{tres} = 2$ g kg^{-1}. This yields for a one segment estuary

$$X_2 = \frac{3}{2} L_e \left(\left(\frac{s_{oc}}{s_{sc}} \right)^{\frac{2}{3}} - \left(\frac{s_{tres}}{s_{sc}} \right)^{\frac{2}{3}} \right). \tag{D4}$$

For an estuary consisting of two segments, Eq. D4 (with $L_e \to L_{e,A}$) is also valid if the salt intrusion is confined to the first segment. In case X_2 is located in segment B, it follows

$$X_2 = L_A + \frac{3}{2} L_{e,B} \left(\left(\frac{s_{oc}}{s_{sc}} \right)^{\frac{2}{3}} - \left(\frac{s_{tres}}{s_{sc}} \right)^{\frac{2}{3}} - \frac{2}{3} \frac{L_A}{L_{e,A}} \right). \tag{D5}$$

These expressions allow for studying the effect of changes to the depth of the entire channel and for changes to the depth of only the downstream segment.

Author contributions. Bouke Biemond: Writing – original draft, Visualization, Validation, Software, Methodology, Investigation, Formal analysis. Wouter Kranenburg: Writing – review & editing. Ymkje Huismans: Writing – review & editing. Huib E. de Swart: Writing – review & editing, Supervision, Funding acquisition. Henk A. Dijkstra: Writing – review & editing, Supervision, Project administration, Funding acquisition. Authors Wouter Kranenburg and Ymkje Huismans contributed equally to this study.

Competing interests. The authors declare that they have no competing interests which are relevant to this study.

Acknowledgements. This work is part of the Perspectief Program SaltiSolutions, which is financed by NWO Domain Applied and Engineering Sciences (2022/TTW/01344701 P18-32 project5) in collaboration with private and public partners. We thank the editor and reviewers for their constructive feedback, which helped to improve the quality of the article.

References

Aristizábal, M. F. and Chant, R. J.: An observational study of salt fluxes in Delaware Bay, Journal of Geophysical Research: Oceans, 120, 2751–2768, https://doi.org/10.1002/2014JC010680, 2015.

Banas, N. S., Hickey, B. M., MacCready, P., and Newton, J. A.: Dynamics of Willapa Bay, Washington: A highly unsteady, partially mixed estuary, Journal of Physical Oceanography, 34, 2413 – 2427, https://doi.org/10.1175/JPO2637.1, 2004.

Bellafiore, D., Ferrarin, C., Maicu, F., Manfè, G., Lorenzetti, G., Umgiesser, G., Zaggia, L., and Levinson, A. V.: Saltwater intrusion in a Mediterranean delta under a changing climate, Journal of Geophysical Research: Oceans, 126, e2020JC016 437, https://doi.org/10.1029/2020JC016437, 2021.

Biemond, B.: Software for 'Dynamics of salt intrusion in complex estuarine networks; an idealised model applied to the Rhine-Meuse Delta' (Version 4.3.6), Zenodo, https://doi.org/10.5281/zenodo.12793378, 2024.

Biemond, B., de Swart, H. E., Dijkstra, H. A., and Díez-Minguito, M.: Estuarine salinity response to freshwater pulses, Journal of Geophysical Research: Oceans, 127, e2022JC018 669, https://doi.org/10.1029/2022JC018669, 2022.

Biemond, B., de Swart, H. E., and Dijkstra, H. A.: Mechanisms of salt overspill at estuarine network junctions explained with an idealized model, Journal of Geophysical Research: Oceans, 128, e2023JC019 630, https://doi.org/10.1029/2023JC019630, 2023.

Biemond, B., de Swart, H. E., and Dijkstra, H. A.: Quantification of salt transports due to exchange flow and tidal flow in estuaries, Journal of Geophysical Research: Oceans, 129, e2024JC021 294, https://doi.org/10.1029/2024JC021294, 2024a.

Biemond, B., Vuik, V., Lambregts, P., de Swart, H. E., and Dijkstra, H. A.: Salt intrusion and effective longitudinal dispersion in man-made canals, a simplified model approach, Estuarine, Coastal and Shelf Science, 298, 108 654, https://doi.org/10.1016/j.ecss.2024.108654, 2024b.

Bowen, M. M. and Geyer, W. R.: Salt transport and the time-dependent salt balance of a partially stratified estuary, Journal of Geophysical Research: Oceans, 108, https://doi.org/10.1029/2001JC001231, 2003.

Bricheno, L. M., Wolf, J., and Sun, Y.: Saline intrusion in the Ganges-Brahmaputra-Meghna megadelta, Estuarine, Coastal and Shelf Science, 252, 107 246, https://doi.org/10.1016/j.ecss.2021.107246, 2021.

Buschman, F. A., Hoitink, A. J. F., van der Vegt, M., and Hoekstra, P.: Subtidal flow division at a shallow tidal junction, Water Resources Research, 46, https://doi.org/10.1029/2010WR009266, 2010.

Chatwin, P.: Some remarks on the maintenance of the salinity distribution in estuaries, Estuarine and Coastal Marine Science, 4, 555–566, https://doi.org/10.1016/0302-3524(76)90030-X, 1976.

Chen, S.-N.: Asymmetric estuarine responses to changes in river forcing: A consequence of nonlinear salt flux, Journal of Physical Oceanography, 45, 2836–2847, https://doi.org/10.1175/JPO-D-15-0085.1, 2015.

Corlett, W. B. and Geyer, W. R.: Frontogenesis at Estuarine Junctions, Estuaries and Coasts, 43, 722–738, https://doi.org/10.1007/s12237-020-00697-1, 2020.

Cox, J. R., Huismans, Y., Knaake, S. M., Leuven, J. R. F. W., Vellinga, N. E., van der Vegt, M., Hoitink, A. J. F., and Kleinhans, M. G.: Anthropogenic Effects on the Contemporary Sediment Budget of the Lower Rhine-Meuse Delta Channel Network, Earth's Future, 9, e2020EF001 869, https://doi.org/10.1029/2020EF001869, 2021.

Davies, A. M. and Jones, J. E.: Sensitivity of Tidal Bed Stress Distributions, Near-Bed Currents, Overtides, and Tidal Residuals to Frictional Effects in the Eastern Irish Sea, Journal of Physical Oceanography, 26, 2553 – 2575, https://doi.org/10.1175/1520-0485(1996)026<2553:SOTBSD>2.0.CO;2, 1996.

de Nijs, M. A. and Pietrzak, J. D.: Saltwater intrusion and ETM dynamics in a tidally-energetic stratified estuary, Ocean Modelling, 49-50, 60–85, https://doi.org/10.1016/j.ocemod.2012.03.004, 2012.

Dijkstra, Y. M. and Schuttelaars, H. M.: A unifying approach to subtidal salt intrusion modeling in tidal estuaries, Journal of Physical Oceanography, 51, 147–167, https://doi.org/10.1175/JPO-D-20-0006.1, 2021.

Eckhaus, W.: Asymptotic analysis of singular perturbations, Elsevier, 2011.

Eslami, S., Hoekstra, P., Kernkamp, H. W. J., Nguyen Trung, N., Do Duc, D., Nguyen Nghia, H., Tran Quang, T., van Dam, A., Darby, S. E., Parsons, D. R., Vasilopoulos, G., Braat, L., and van der Vegt, M.: Dynamics of salt intrusion in the Mekong Delta: results of field observations and integrated coastal–inland modelling, Earth Surface Dynamics, 9, 953–976, https://doi.org/10.5194/esurf-9-953-2021, 2021.

Garcia, A. M. P., Geyer, W. R., and Randall, N.: Exchange Flows in Tributary Creeks Enhance Dispersion by Tidal Trapping, Estuaries and Coasts, 45, 363–381, https://doi.org/10.1007/s12237-021-00969-4, 2022.

Geyer, W. R. and MacCready, P.: The estuarine circulation, Annual Review of Fluid Mechanics, 46, 175–197, https://doi.org/10.1146/annurev-fluid-010313-141302, 2014.

Geyer, W. R. and Signell, R. P.: A reassessment of the role of tidal dispersion in estuaries and bays, Estuaries, 15, 97–108, https://doi.org/10.2307/1352684, 1992.

Godin, G.: Compact approximations to the bottom friction term, for the study of tides propagating in channels, Continental Shelf Research, 11, 579–589, https://doi.org/10.1016/0278-4343(91)90013-V, 1991.

Godin, G.: The propagation of tides up rivers with special considerations on the upper Saint Lawrence River, Estuarine, Coastal and Shelf Science, 48, 307–324, https://doi.org/10.1006/ecss.1998.0422, 1999.

Gong, W., Maa, J. P.-Y., Hong, B., and Shen, J.: Salt transport during a dry season in the Modaomen Estuary, Pearl River Delta, China, Ocean & coastal management, 100, 139–150, https://doi.org/10.1016/j.ocecoaman.2014.03.024, 2014.

Huismans, Y. and Plieger, R.: Verondieping Oude Maas als potentiele maatregel tegen verzilting: een verkenning, Tech. rep., Deltares, 11202241-003-ZWS-0003 (In Dutch), 2019.

Huismans, Y., Leummens, L., Rodrigo, S., Laan, S., Kranenburg, W., and van der WIjk, R.: Extra debiet over stuw Hagestein voor het tegengaan van verzilting van de Lek, Tech. rep., Deltares, 11210363-001-ZKS-0001 (In Dutch), 2024.

Kolb, P., Zorndt, A., Burchard, H., Gräwe, U., and Kösters, F.: Modelling the impact of anthropogenic measures on saltwater intrusion in the Weser estuary, Ocean Science, 18, 1725–1739, https://doi.org/10.5194/os-18-1725-2022, 2022.

Kranenburg, W., Van der Kaaij, T., Tiessen, M., Friocourt, Y., and Blaas, M.: Salt intrusion in the Rhine Meuse Delta: Estuarine circulation, tidal dispersion or surge effect, in: Proceedings of the 39th IAHR World Congress. June. Granada, Spain, pp. 5601–5608, https://doi.org/10.3850/IAHR-39WC2521711920221058, 2022.

Laan, S., Chavarrias, V., Huismans, Y., and van der Wijk, R.: Verzilting Hollandsche IJssel en Lek, Tech. rep., Deltares, 11206830-017-ZWS-0001 (In Dutch), 2021.

Laan, S., Huismans, Y., Rodrigo, S., Leummens, L., and Kranenburg, W.: Effect bodemligging op verzilting Nieuwe Waterweg, Nieuwe Maas en Lek, Tech. rep., Deltares, 11208075-010-ZWS-0001 (In Dutch), 2023.

Liu, C., Yu, M., Jia, L., Cai, H., and Chen, X.: Impacts of physical alterations on salt transport during the dry season in the Modaomen Estuary, Pearl River Delta, China, Estuarine, Coastal and Shelf Science, 227, 106 345, https://doi.org/10.1016/j.ecss.2019.106345, 2019.

Liu, J., Hetland, R., Yang, Z., Wang, T., and Sun, N.: Response of salt intrusion in a tidal estuary to regional climatic forcing, Environmental Research Letters, https://doi.org/10.1088/1748-9326/ad4fa1, 2024.

715 MacCready, P.: Toward a unified theory of tidally-averaged estuarine salinity structure, Estuaries, 27, 561–570, https://doi.org/10.1007/BF02907644, 2004.

MacCready, P.: Estuarine adjustment, Journal of Physical Oceanography, 37, 2133–2145, https://doi.org/10.1175/JPO3082.1, 2007.

MacVean, L. J. and Stacey, M. T.: Estuarine Dispersion from Tidal Trapping: A New Analytical Framework, Estuaries and Coasts, 34, 45–59, https://doi.org/10.1007/s12237-010-9298-x, 2011.

720 Maicu, F., De Pascalis, F., Ferrarin, C., and Umgiesser, G.: Hydrodynamics of the Po River-Delta-Sea System, Journal of Geophysical Research: Oceans, 123, 6349–6372, https://doi.org/10.1029/2017JC013601, 2018.

Martyr-Koller, R., Kernkamp, H., van Dam, A., van der Wegen, M., Lucas, L., Knowles, N., Jaffe, B., and Fregoso, T.: Application of an unstructured 3D finite volume numerical model to flows and salinity dynamics in the San Francisco Bay-Delta, Estuarine, Coastal and Shelf Science, 192, 86–107, https://doi.org/10.1016/j.ecss.2017.04.024, 2017.

725 Monismith, S.: An integral model of unsteady salinity intrusion in estuaries, Journal of Hydraulic Research, 55, 392–408, https://doi.org/10.1080/00221686.2016.1274682, 2017.

Monismith, S., Kimmerer, W., Burau, J., and Stacey, M.: Structure and flow-induced variability of the subtidal salinity field in northern San Francisco Bay, Journal of physical Oceanography, 32, 3003–3019, https://doi.org/10.1175/1520-0485(2002)032<3003:SAFIVO>2.0.CO;2, 2002.

730 Moriasi, D. N., Gitau, M. W., Pai, N., and Daggupati, P.: Hydrologic and water quality models: Performance measures and evaluation criteria, Transactions of the ASABE, 58, 1763–1785, https://doi.org/10.13031/trans.58.10715, 2015.

Murray, A. B.: Contrasting the goals, strategies, and predictions associated with simplified numerical models and detailed simulations, Geophysical Monograph-American Geophysical Union, 135, 151–168, https://doi.org/10.1029/135GM11, 2003.

Nash, J. and Sutcliffe, J.: River flow forecasting through conceptual models part I — A discussion of principles, Journal of Hydrology, 10, 735 282–290, https://doi.org/10.1016/0022-1694(70)90255-6, 1970.

Nguyen, A. D. and Savenije, H. H.: Salt intrusion in multi-channel estuaries: a case study in the Mekong Delta, Vietnam, Hydrology and Earth System Sciences, 10, 743–754, https://doi.org/10.5194/hess-10-743-2006, 2006.

Okubo, A.: Effect of shoreline irregularities on streamwise dispersion in estuaries and other embayments, Netherlands Journal of Sea Research, 6, 213–224, https://doi.org/10.1016/0077-7579(73)90014-8, 1973.

740 Pritchard, D. W.: A study of the salt balance in a coastal plain estuary, Journal of Marine Research, 13, 133–144, 1954.

Qiu, C. and Zhu, J.: Assessing the Influence of Sea Level Rise on Salt Transport Processes and Estuarine Circulation in the Changjiang River Estuary, Journal of Coastal Research, 31, 661 – 670, https://doi.org/10.2112/JCOASTRES-D-13-00138.1, 2015.

Qiu, C. and Zhu, J.-R.: Influence of seasonal runoff regulation by the Three Gorges Reservoir on saltwater intrusion in the Changjiang River Estuary, Continental Shelf Research, 71, 16–26, https://doi.org/10.1016/j.csr.2013.09.024, 2013.

745 Ralston, D. K. and Geyer, W. R.: Response to Channel Deepening of the Salinity Intrusion, Estuarine Circulation, and Stratification in an Urbanized Estuary, Journal of Geophysical Research: Oceans, 124, 4784–4802, https://doi.org/10.1029/2019JC015006, 2019.

Ralston, D. K., Geyer, W. R., and Lerczak, J. A.: Structure, variability, and salt flux in a strongly forced salt wedge estuary, Journal of Geophysical Research: Oceans, 115, https://doi.org/10.1029/2009JC005806, 2010.

Savenije, H. H.: Predictive model for salt intrusion in estuaries, Journal of Hydrology, 148, 203–218, https://doi.org/10.1016/0022-750 1694(93)90260-G, 1993.

Scully, M. E. and Geyer, W. R.: The Role of Advection, Straining, and Mixing on the Tidal Variability of Estuarine Stratification, Journal of Physical Oceanography, 42, 855 – 868, https://doi.org/10.1175/JPO-D-10-05010.1, 2012.

Siles-Ajamil, R., Díez-Minguito, M., and Losada, M.: Tide propagation and salinity distribution response to changes in water depth and channel network in the Guadalquivir River Estuary: An exploratory model approach, Ocean & Coastal Management, 174, 92–107, https://doi.org/10.1016/j.ocecoaman.2019.03.015, 2019.

Walters, R.: A model for tides and currents in the English Channel and southern North Sea, Advances in Water Resources, 10, 138–148, https://doi.org/10.1016/0309-1708(87)90020-0, 1987.

Wang, J., de Swart, H. E., and Dijkstra, Y. M.: Dependence of tides and river water transport in an estuarine network on river discharge, tidal forcing, geometry and sea level rise, Continental Shelf Research, 225, 104 476, https://doi.org/10.1016/j.csr.2021.104476, 2021.

Warner, J., Schoellhamer, D., Burau, J., and Schladow, G.: Effects of tidal current phase at the junction of two straits, Continental Shelf Research, 22, 1629–1642, https://doi.org/10.1016/S0278-4343(02)00026-2, proceedings from the Tenth Biennial Conference on the Physics of Estuaries and Coastal Seas, 2002.

Wei, X., Schramkowski, G. P., and Schuttelaars, H. M.: Salt dynamics in well-mixed estuaries: Importance of advection by tides, Journal of Physical Oceanography, 46, 1457–1475, https://doi.org/10.1175/JPO-D-15-0045.1, 2016.

Wei, X., Williams, M. E., Brown, J. M., Thorne, P. D., and Amoudry, L. O.: Salt Intrusion as a Function of Estuary Length in Periodically Weakly Stratified Estuaries, Geophysical Research Letters, 49, e2022GL099 082, https://doi.org/10.1029/2022GL099082, 2022.

Winterwerp, J. C.: Decomposition of the mass transport in narrow estuaries, Estuarine, Coastal and Shelf Science, 16, 627–638, https://doi.org/10.1016/0272-7714(83)90075-6, 1983.

Wu, S., Cheng, H., Xu, Y., Li, J., and Zheng, S.: Decadal changes in bathymetry of the Yangtze River Estuary: Human impacts and potential saltwater intrusion, Estuarine, Coastal and Shelf Science, 182, 158–169, https://doi.org/10.1016/j.ecss.2016.10.002, 2016.

Wullems, B. J. M., Brauer, C. C., Baart, F., and Weerts, A. H.: Forecasting estuarine salt intrusion in the Rhine–Meuse delta using an LSTM model, Hydrology and Earth System Sciences, 27, 3823–3850, https://doi.org/10.5194/hess-27-3823-2023, 2023.

Xue, P., Chen, C., Ding, P., Beardsley, R. C., Lin, H., Ge, J., and Kong, Y.: Saltwater intrusion into the Changjiang River: A model-guided mechanism study, Journal of Geophysical Research: Oceans, 114, https://doi.org/10.1029/2008JC004831, 2009.

Zhang, E., Savenije, H. H., Wu, H., Kong, Y., and Zhu, J.: Analytical solution for salt intrusion in the Yangtze Estuary, China, Estuarine, Coastal and Shelf Science, 91, 492–501, https://doi.org/10.1016/j.ecss.2010.11.008, 2011.

Zhu, J., Ding, P., Zhang, L., Wu, H., and Cao, H.: Influence of the deep waterway project on the Changjiang Estuary, in: The environment in Asia Pacific harbours, pp. 79–92, Springer, https://doi.org/10.1007/1-4020-3655-8_6, 2006.